



2010-03-17

Optimal Design of a Planar 3-RPR Haptic Interface Based on Manipulability

Wesley Kay Harris

Brigham Young University - Provo

Follow this and additional works at: <https://scholarsarchive.byu.edu/etd>



Part of the [Mechanical Engineering Commons](#)

BYU ScholarsArchive Citation

Harris, Wesley Kay, "Optimal Design of a Planar 3-RPR Haptic Interface Based on Manipulability" (2010). *All Theses and Dissertations*. 2050.

<https://scholarsarchive.byu.edu/etd/2050>

This Thesis is brought to you for free and open access by BYU ScholarsArchive. It has been accepted for inclusion in All Theses and Dissertations by an authorized administrator of BYU ScholarsArchive. For more information, please contact scholarsarchive@byu.edu, ellen_amatangelo@byu.edu.

Optimal Design of a Planar 3-RPR Haptic
Interface Based on Manipulability

Wesley K. Harris

A thesis submitted to the faculty of
Brigham Young University
in partial fulfillment of the requirements for the degree of
Master of Science

Mark B. Colton, Chair
Walter E. Red
Christopher A. Mattson

Department of Mechanical Engineering
Brigham Young University
Thesis Completed April 2010

Copyright © 2010 Wesley K. Harris

All Rights Reserved

ABSTRACT

Optimal Design of a Planar 3-RPR Haptic Interface Based on Manipulability

Wesley K. Harris

Department of Mechanical Engineering

Master of Science

A haptic interface is a robotic force feedback device that provides a sense of touch to users of virtual reality simulations. This thesis presents a general method for the design optimization of parallel planar haptic devices based on maximizing the manipulability of the interface over its workspace. Manipulability is selected as the key design objective to ensure avoidance of singular configurations within the workspace and to maximize the interface's ability to generate feedback forces and torques in each direction in each handle location and orientation.

The optimization approach developed in this thesis results in a set of candidate designs that are found by stepping the design parameters through the range of possible values, and testing the manipulability and other measures (including workspace area and space) at each location and orientation of the interface handle. To find the optimal design, a multi-objective approach is taken to generate a set of Pareto optimal designs. A smart Pareto filter is employed to yield a smaller set of designs representative of the full Pareto frontier. The most desirable design is chosen from this reduced set. The result is a general optimization method applicable to parallel haptic interfaces. The method is demonstrated on the design of a 3-RPR parallel planar interface.

Keywords: Wesley Harris, haptic, manipulability, singularity avoidance, multi-objective optimization, parallel, planar, RPR.

ACKNOWLEDGMENTS

Special thanks go to Dr. Mark Colton for his enthusiasm, guidance, insights, patience, and confidence. His time and resources made this thesis possible. I thank my committee for their time and critiques, especially Dr. Mattson for his excellent optimization input. Finally, I thank my wife Jennifer for her love, support, motivation, and belief in me.

TABLE OF CONTENTS

LIST OF TABLES vii

LIST OF FIGURES ix

1 Introduction..... 11

1.1 Overview..... 11

1.2 Haptic Interfaces 12

1.3 Related Work 16

1.3.1 Parallel Manipulators 16

1.3.2 Optimization of Parallel Manipulators..... 18

1.3.3 Design of Haptic Interfaces..... 20

1.4 Scope and Contribution of the Thesis..... 21

1.4.1 Contributions..... 21

1.5 Organization of the Thesis 22

2 Modeling 25

2.1 Overview..... 25

2.2 3-RPR Mechanism 26

2.3 Position Kinematics 27

2.3.1 Kinematic Equations 28

2.3.2 Inverse Kinematics..... 29

2.3.3 Forward Kinematics 30

2.4 Velocity Kinematics 32

2.4.1 Jacobian..... 33

2.4.2 Statics 34

2.5 Singularities and Manipulability..... 34

3	Optimization Method.....	43
3.1	Overview.....	43
3.2	Selection of Base Configurations	46
3.2.1	Selection of Base P	47
3.2.2	Search Limits	48
3.2.3	Selection of Base Q	48
3.2.4	Selection of Base R	49
3.2.5	Total Search Region.....	51
3.3	Mapping Manipulability	52
3.3.1	Constraints	52
3.4	Identification and Separation of the Workspaces	58
3.5	Characterization of Workspaces	59
3.6	Workspace Optimization	61
3.6.1	Optimization Problem Statement	62
3.6.2	Pareto Filter Optimization.....	64
3.7	Software: Optimization Algorithm Implementation.....	70
4	Results	71
5	Discussion and Conclusions	83
5.1	Discussion.....	83
5.2	Conclusions.....	84
5.3	Future Research	87
	References	89
	Appendix.....	93

LIST OF TABLES

Table 4-1: Geometry Arguments for Optimization	71
Table 4-2: Optimization Settings	72
Table 4-3: Filtered and Optimized Designs	73
Table 4-4: Visualization of Filtered Designs	75
Table 4-5: Characteristics of Filtered Designs.....	77
Table 4-6: Characteristics as a Percentage of Filtered Design Winners	78
Table 4-7: Design Area Values.....	78
Table 4-8: Visualization of Design Configurations.....	79
Table 4-9: Design Configuration Data.....	81
Table 4-10: Closer Look at Two Selected Designs	82

LIST OF FIGURES

Figure 1-1: Planar 3-RPR Parallel Mechanism.....	16
Figure 2-1: Planar 3-RPR Parallel Mechanism.....	28
Figure 2-2: Two-bar Mechanism	37
Figure 2-3: Manipulability Measure on a Simple Two-bar Mechanism.....	37
Figure 2-4: Manipulability Measure Graphs for a Two-bar Mechanism.....	38
Figure 2-5: Manipulability Map With $\phi = 0$ for a Planar 3-RPR Parallel Mechanism	39
Figure 2-6: Singularity Configuration for Planar 3-RPR Parallel Mechanism.....	40
Figure 2-7: Manipulability Map of 3-RPR Manipulator With $\phi = 45^\circ$	41
Figure 3-1: Planar 3-RPR Parallel Mechanism.....	44
Figure 3-2: General Optimization Method Flow Chart	45
Figure 3-3: Placement of Base P.....	47
Figure 3-4: Outer Constraint of Second Base Placement	48
Figure 3-5: Placement of Base Q.....	49
Figure 3-6: Placement of Base R	50
Figure 3-7: Movement of Handle, H.....	51
Figure 3-8: Interior Joint Length Constraints	53
Figure 3-9: ϕ Constraints, $\phi = 0^\circ$	54
Figure 3-10: ϕ Constraints, $\phi = 90^\circ$	54
Figure 3-11: One Fully Constrained Design.....	56
Figure 3-12: Post-Constraint Sample Region to be Measured.....	57
Figure 3-13: Manipulability Map of Post-constraint Sample Region.....	57
Figure 3-14: Singularity Discovery in the Manipulability Map	58
Figure 3-15: Identification and Separation of Workspaces	59

Figure 3-16: Understanding Compactness.....	60
Figure 3-17: Area and Perimeter Derivation	61
Figure 3-18: Pareto and Smart Pareto Filters.....	66
Figure 3-19: Visualization of Trade-offs and Filtered Designs.....	68
Figure 3-20: Reducing Designs Subject to a Constraint.....	69
Figure 3-21: Representation of an Optimized Haptic Design Interface	69
Figure 4-1: Pareto and Smart Pareto Filter Results	74

1 INTRODUCTION

1.1 Overview

Haptic simulations enable a user to connect with a virtual environment via the sense of touch. Haptic interfaces are robotic force and torque feedback devices that provide this sense of touch to users. These types of interfaces are becoming more prevalent in simulation applications such as design, art, medicine, and gaming. The end goal of haptic research is to provide a realistic *feel* or experience to the user. The need for interfaces with better capabilities increases as more demanding applications are developed.

The current and future needs in haptic interfaces are under served. Current haptic interfaces have several limitations in hardware (bandwidth, force capabilities, resolution, portability, etc.), software (haptic refresh rates, collision detection, etc.), graphics (refresh rates, detail, etc.), and control (stability, tracking, etc.) [1]. These limitations decrease the feeling of realism that a user can experience.

For a user to have an immersive experience each of these challenges must be addressed. This thesis addresses the design of hardware interfaces, with the specific goal of improving force capabilities. The approach taken in this work to overcome these limitations is to employ an interface design that incorporates high force, high bandwidth linear motors. A parallel kinematic configuration, as compared to a serial kinematic configuration, has the advantage of higher

stiffness, higher payload capacity, and lower inertia with the inherent cost of a more complex mechanism and a reduction in workspace [2].

This thesis addresses the challenge of designing a parallel haptic interface with the ability to provide to the user uniform force and torque feedback, incorporating high-force, high-bandwidth motors to provide a more realistic immersive haptic experience. This thesis demonstrates an optimization method to design the kinematic configuration of a 3-RPR planar parallel haptic interface to maximize its workspace and manipulability, which is a measure of the device's ability to generate forces and torques at each point in the workspace. The optimization process involves:

1. the kinematic and static modeling of a 3-RPR (3-degree of freedom revolute/prismatic/revolute) parallel-planar haptic mechanism;
2. the determination of a manipulability measure map for each design of the parallel interface;
3. the identification and characterization of viable workspaces;
4. the selection of an optimal design based on the “best” workspace, as determined by area, shape, and manipulability.

An explanation of each of these points follows in subsequent sections. Prior to this explanation a few points will be discussed: an overview of haptic interfaces, followed by key concepts related to their design, and an overview of related work.

1.2 Haptic Interfaces

Haptic interfaces belong to a special category of devices that allow a user to interact with a virtual environment. Haptic interfaces are input/output devices. In most cases, a user

manipulates the haptic interface, which typically sends position and orientation information to the computer. The computer updates the virtual environment to reflect the motion of the human user, computes interaction forces and torques that the user should feel as a result of his interaction with the virtual environment, and sends the interaction forces back to the haptic interface, which exerts the appropriate forces and torques on the user. An example of a haptic interface is a flight simulator with motion simulation capabilities. As the pilot manipulates the joystick, the simulator creates motion feedback to create the illusion of actual flight. In this case the entire apparatus functions as a haptic device.

Whatever the specific simulation, the realism of the haptic experience will depend on many factors. The best software, physical modeling, and computer graphics will fail to provide a user with a completely realistic experience if the capabilities of the interface hardware fail to convey force and torque information to the user in a timely and accurate manner.

Different interface configurations have different attributes. A large number of haptic interfaces are designed as serial kinematic chains, which means that the links are connected one to another, end to end, from the base to the end-effector. The human arm is an example of a serial link manipulator. The shoulder acts as a base and each joint is connected serially until the tips of the fingers.

There are advantages and disadvantages to the use of serial devices. One distinct advantage of serial designs is that it is relatively easy to find a space in which an interface end-effector can exert uniform force and torque on a user. The measure of a mechanism's ability to provide uniform force and torque is referred to as manipulability. The concept of manipulability is discussed in detail in subsequent sections.

Although serial interfaces have positive manipulability characteristics, they also have a number of attributes that make their use in haptic modeling a challenge. Due to the nature of their construction small motors are employed at the joints of serial devices. In many cases it is impractical, for reasons related to weight and geometry, to have large motors located at each joint. Large motors can hamper the movement of the device and the increased weight can reduce the dynamic capabilities of the device. Due to these limitations, small motors are typically employed in haptic devices with a resulting decrease in force, torque, and bandwidth capabilities of the interface. The human hand gives insight into the challenges of actuating serial manipulators: instead of relying on actuators located at each joint of each finger, a system of tendons is used to operate the tips of the fingers while the muscles that operate them are located further back.

An alternate method of configuring a device is to place the links in parallel. A device is in parallel if its kinematic chain is a closed loop. This results in an end-effector that is supported by more than one joint. The benefits of parallel manipulators are compelling. As each link attaches to the end-effector directly from the base, larger motors can be effectively utilized. The result of using high-force motors at each joint is an end-effector that can deliver to a user more realistic feedback quickly and accurately by employing high bandwidth and high force-torque.

Parallel manipulators also present certain drawbacks that make their implementation as haptic interfaces challenging. One of these drawbacks is related to how the physical setup of an interface affects its ability to exert force on an end effector. As an end effector moves through its workspace the ability of the interface to exert desired forces and torques on the end effector changes. Restated, the forces and torques exerted on the end effector depend on the motors' positions and orientations in relation to the end effector. As mentioned previously, the ability of

an interface to exert forces on the end effector uniformly in all directions is known as manipulability. One of the challenges with the use of parallel devices as haptic interfaces is the difficulty of designing parallel devices in such a way that the end effector can move through its workspace without encountering areas of low manipulability, which are areas in which an interface is less able to deliver desired forces or torques to a user in at least one direction.

In both serial and parallel devices there are sometimes configurations in a device's workspace in which the manipulability is zero. In these singular configurations, the interface loses the ability to provide force or torque feedback to the user in at least one direction. This is equivalent to losing a degree of freedom.

It is more difficult to design parallel devices to avoid singularities than it is to design serial devices, due to the interconnected nature of the parallel device. The task is to design a parallel haptic interface that will provide a sufficiently large workspace with the desired size, shape, and manipulability characteristics. The focus of this thesis is to present a general method to determine the design for an interface that will provide an optimal workspace that is free of singularities.

To demonstrate the method this thesis explores the optimal design of a specific type of parallel planar device. This device consists of three linear motors connected to the end effector or handle of the interface in a parallel configuration, as shown in Figure 1-1. The design of the interface is altered by changing the location of the motor base points P , Q , and R . The telescoping or prismatic joints of the linear motors, combined with the rotational or revolute joints located at the ends of each of the motors, permit translational and rotational movement of the handle H within the plane.

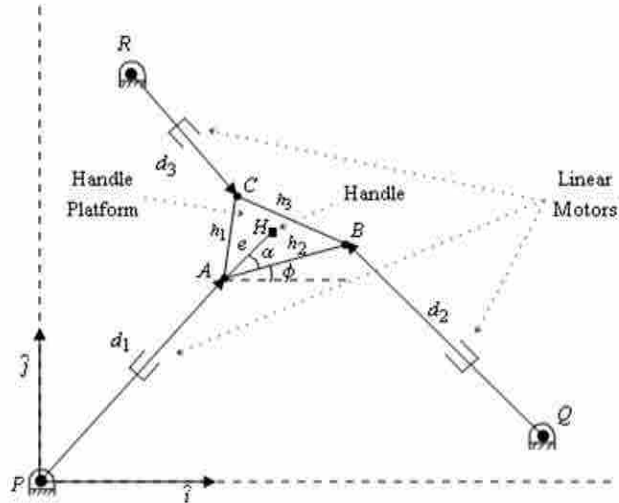


Figure 1-1: Planar 3-RPR Parallel Mechanism

The general method applied to find the optimal locations of the bases is the principal discussion of this thesis and is demonstrated in detail in subsequent sections. First, a summary discussion of methods used in designing related devices will be presented.

1.3 Related Work

1.3.1 Parallel Manipulators

Parallel manipulators have several advantages over serial manipulators, including high stiffness, low inertia, and good dynamic characteristics [2]. Disadvantages include limited workspace, difficulties in their analysis, synthesis, control and trajectory planning; their direct or forward kinematics are also typically challenging [2]. Numerous papers addressed the design and kinematics of parallel manipulators:

- Ji and Wu study an efficient approach to the forward kinematics of a 3-RPR manipulator [3].

- Sadjadian and Taghirad determine the forward and inverse kinematics of a hydraulic shoulder parallel manipulator. The solution is verified by trajectory simulations in the workspace [4].
- Unal et al. examine a 2-DOF five bar linkage device, optimizing kinematic and dynamic considerations for a haptic application [5].
- Christiansson and Fritz improved a device-specific performance measure in a 3-DOF haptic device [6].
- Wang and Hayward did a redesign and performance evaluation of a 2-DOF parallel haptic manipulator. Their work focused on improvement of the dynamic considerations [7].
- Frisoli et al. designed a 2-DOF haptic device for improved kinematic and dynamic performance over a given workspace [8].
- Stocco et al. develop a novel approach based on isotropic considerations to select design parameters for parallel devices; they show proposed extensions to haptic applications [9].

The 3-RPR device, which is the test manipulator used in this thesis, has been studied and constructed by multiple researchers:

- Williams and Joshi constructed a pneumatic 3-RPR device to study pneumatic parallel manipulator control [10].
- Zein et al. search for maximal joint space singularity-free boxes working towards determination of joint limit and link length selection [11].

- Li et al. guarantee singularity-free cylindrical zones in the workspace without discretization; they demonstrate that a smaller range of ϕ will increase the workspace [12].
- Yang and O'Brien design a 3- RPR manipulator, using the third base joint as the design variable, to find singularity-free workspaces [13].
- Gallant and Boudreau adjust architecture parameters to match usable workspace to a prescribed workspace and then take singularities into consideration. They employ a genetic algorithm to aid in optimization of the fit to prescribed workspace and the end-effector's dexterity [14].

1.3.2 Optimization of Parallel Manipulators

Optimization of parallel manipulators is a topic of particular interest to researchers, although the goal and methods of each researcher differ. While parallel manipulators have several advantages, there are also trade-offs. One of the primary challenges with the use of a parallel manipulator is the appearance of singularities in the workspace and consequently small workspace areas. Tyapin et al. optimized a specific parallel manipulator to avoid unreachable areas using a geometric approach [15]. Other researchers have addressed the problem of singularity avoidance. Masouleh and Gosselin used a 3-PRR device to avoid singularities, although this research did not focus on maximizing the workspace [16]. Alici and Shirinzadeh optimized a revolute jointed linkage based on kinematic isotropy and force balancing [17]. Gallant and Boudreau used an RPR device to study optimal singularity-free workspaces. They optimized their architectural parameters so that a manipulator's workspace would match a prescribed workspace [14]. Yang and O'Brien used one of the device bases of an RPR

manipulator as a design variable and identified and categorized singularities for different designs [13]. Li and Richard found circular singularity-free zones within the workspace of an RPR manipulator [12]. Their research showed that increasing the rotational range of the planar end-effector reduces the size of the singularity free zone. Additional research has been done to achieve optimal singularity avoidance in the end-effector workspace:

- Lee relates that the commonly used measure of manipulability, the manipulability ellipsoid, does not transform the exact joint velocity constraints into task space and performs research to improve this measure using a polytope approach [18].
- Doty et al. study fundamental problems with commonly used dexterous measures of robot manipulators [19].
- Voglewede and Ebert-Uphoff provide a framework to compare existing methods and create new methods to measure stiffness-loss/singularities [20].
- Liu et al. analyze a spatial 3-DOF manipulator including identification of three types of singularities [21].
- Gosselin and Angeles design a 3-DOF RRR manipulator for kinematic considerations including: symmetry, existence of a non-vanishing workspace for all orientations of the end-effector, maximization of the workspace, and consideration of the isotropy of the Jacobian of the manipulator [22].
- Gosselin and Wang analyze a special Spherical 3-DOF parallel mechanism with revolute actuators. They use forward and inverse kinematics to examine singularities [23].

- Liu develops a design method to optimize kinematic considerations applying performance charts: comparing design performance with desired workspace characteristics [24].

1.3.3 Design of Haptic Interfaces

There are a wide variety of haptic interfaces. These interfaces vary according to their application. Many of these haptic devices are of the serial arm type, such as the Phantom Premium 1.5 [25]. Parallel interfaces are also used, such as the popular gaming Novint Falcon [26] and the Force Dimension Delta [27]. All of the many manipulators created for use in virtual environments have a common goal: to give the user a haptic interaction with that environment.

In order to better accomplish this goal research has been conducted to optimize many facets of haptic interfaces. Gosselin et al. placed emphasis on requirements unique to a Computer Aided Design or virtual sculpting device; the device used geometric and static optimization [28]. Vlachos and Papadopoulos focus on optimizing the transparency (the absence of haptic device-induced parasitic torques/forces during motion) of a haptic device [29]. Christiansson and Fritz optimized a haptic device based on a stiff master and compliant slave to improve teleoperation performance in 1-DOF [6]. An additional example is that of Unal et al., who took a general approach to the optimization of haptic interfaces with respect to multiple objectives, including kinematic and dynamic criteria; they use Pareto filter optimization [5].

From the body of research it is evident that a large number of design objectives are present in haptic devices. The research indicates that much has been done to address these issues. Even more work must be done to align a user with an immersive haptic experience; in particular the maximization of a singularity-free workspace with acceptable levels of manipulability is an area that requires further exploration.

1.4 Scope and Contribution of the Thesis

As discussed in previous sections, there are many approaches to solving the limitations associated with robotic devices and, in particular, haptic devices. This thesis extends the current body of work by presenting a general method for singularity-avoidance optimization with respect to manipulability maximization and geometry design objectives for parallel haptic devices.

1.4.1 Contributions

A singularity-avoidance/manipulability-maximization (SAMM) approach to design of a parallel haptic interface configuration is presented, with the major contributions being:

1. A mathematical model of a 3-RPR (3-degree of freedom revolute-prismatic-revolute) parallel-planar mechanism is presented. This device serves as the test case in this thesis for demonstration of the SAMM method used to design parallel haptic interfaces. This design can be used for the construction of the described device for future haptic research.
2. Development of the SAMM method for the optimal design of parallel haptic interfaces based on manipulability and singularity avoidance. This method can be modified to include design objectives in addition to manipulability and geometric workspace characteristics. The method can also be expanded to include more complex interfaces.
3. Implementation of the SAMM optimization method on a 3-RPR parallel-planar device. This method includes the determination of a manipulability measure map for each configuration of the parallel interface and includes the identification and characterization of viable workspaces. The final step in the method is the selection of

an optimal design based on the “best” workspace, where best is determined by the designer based on the combination of characteristics desired.

4. Development of a software tool to alter the desired characteristics of a workspace, enabling the selection of alternate designs. A user can use the software to select a workspace and hence a design with the characteristics they desire; for example, more emphasis can be placed on shape than size or on manipulability characteristics versus size.

These contributions are a first step towards the optimal design of a haptic interface. This method is used to generate feasible designs based on singularity avoidance, static force capabilities, and manipulability. To fully optimize a haptic interface other factors must be considered, such as the interface dynamics, to provide a user with an accurate representation of realism.

1.5 Organization of the Thesis

Chapter 2 describes the process of modeling the 3-RPR parallel planar interface that is analyzed in this thesis. After a brief overview the discussion focuses on obtaining the position kinematics and the velocity kinematics followed by the derivation of the singularities and manipulability of the interface.

Chapter 3 focuses on the core of the thesis. This chapter discusses in detail the general method used to select an optimal design using as a demonstration of the method the device modeled in Chapter 2. The chapter addresses selection of base configurations, mapping manipulability, identification and separation of the workspaces, characterization of workspaces, evaluation of workspaces and workspace selection, with some final comments on the implementation of the optimization algorithm in software.

Chapter 4 examines the results of the general method as applied to a 3-RPR parallel planar interface.

Chapter 5 contains an in-depth discussion of the results found in Chapter 4, followed by conclusions and recommendations for future research.

2 MODELING

2.1 Overview

The modeling objectives for the 3-RPR parallel planar haptic interface include:

- Development of a basic parameterized design
- Derivation of forward and inverse position kinematics
- Derivation of forward and inverse velocity kinematics
- Determination of Jacobian and static force model
- Derivation of manipulability measure

To find the optimal design, it is necessary to derive the position and velocity kinematics of the 3-RPR device, which are used to determine the manipulability of the device as the end effector moves through its total workspace. This region is defined by the maximum reach of the end effector in all directions of the plane, constrained by the physical characteristics of the system (location of motor bases and length of handle and linear motors). The map of the manipulability over this region is used to divide the region into singularity-free workspaces. The characteristics for each workspace are determined. These characteristics include the measure of the workspace manipulability and the workspace size and shape. After the relevant information is recorded the design is altered by changing the location of the bases. This process is repeated until all desired designs have been tested.

The value of each design or configuration of the motors is judged on the singularity-free region or workspace that it creates. The workspace is valued based on its size, shape, mean manipulability, and standard deviation of manipulability. The selection of an optimal workspace is discussed in Chapter 3. The optimal interface design is the one that results in the optimal workspace, based on the measures discussed previously.

For a haptic device to be effective, both its position and velocity kinematics must be known. The forward kinematic equations are particularly important for a haptic device as they are used by the computer to determine the handle location and orientation, which serve as the input to the virtual environment. The forward kinematics of a parallel interface are typically more difficult to derive than the inverse kinematics, which is the opposite of the serial case, for which it is typically more difficult to derive the inverse kinematics [2].

The process of finding the kinematic equations is outlined below. Once the kinematic equations have been derived, it is possible to measure the manipulability of the interface. This chapter concludes with a description of manipulability, how it is obtained, and how it is employed in this project.

2.2 **3-RPR Mechanism**

Many different configurations of planar parallel manipulators are possible. The manipulator to be designed in this project has three degrees of freedom and three actuated prismatic joints connected to the ground and end effector via passive revolute joints. This set up is abbreviated as 3-RPR. The letter P (prismatic) is underlined to indicate that it is the actuated joint and the lack of the underline under the other joints, labeled with the letter R (revolute), indicates that they are passive (unactuated). This configuration provides significant force, high

stiffness, and fast response times to the user. A detailed look at the device follows in the position kinematics.

2.3 Position Kinematics

The forward and inverse kinematic equations of a parallel 3-RPR manipulator have been studied by several researchers [3] [4][30]. For the proposed interface, inverse kinematic equations are used to solve for the joint lengths when the coordinates of the handle are given. For parallel manipulators deriving the inverse kinematic equations is a relatively easy process and an analytical solution can often be found. The forward or direct kinematic equations are used to find the handle coordinates when the lengths of the joint variables are given or measured. Unlike serial robots, this is a difficult problem for parallel manipulators. Several solutions are possible and these are typically only obtained using numerical methods.

Figure 2-1 contains a schematic of the proposed model. Points P , Q , and R are the bases attached to the plane. The variables d_1 , d_2 , and d_3 are the lengths of the prismatic joints connecting the base to the movable handle platform ABC . The end effector is a handle, point H , on the movable platform. The location of the handle on the movable platform is defined by e and α . Each location, length and angle is adjustable, providing a designer the ability to perform additional future optimizations. Input for the forward kinematics is given as the set of joint variables \mathbf{q} , where $\mathbf{q} = [d_1 \ d_2 \ d_3]^T$. In a haptics application, these values would be measured using linear encoders. The handle variables $\mathbf{x} = [x_H \ y_H \ \phi]^T$ are calculated from the forward kinematic equations.

Put simply the kinematic equations yield the relationship between all the components of the interface. Forward kinematic equations allow calculation of handle variables, given the

measured joint variables (motor lengths). The handle variables then serve as inputs to the virtual environments.

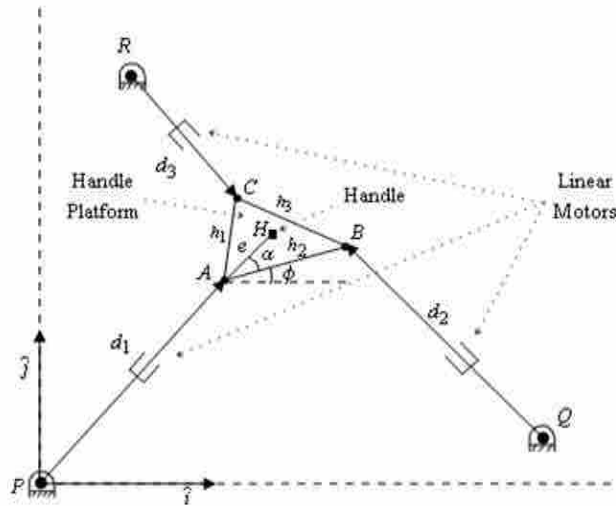


Figure 2-1: Planar 3-RPR Parallel Mechanism

2.3.1 Kinematic Equations

The position kinematic equations of the model developed by the author are derived in this section. These equations provide the basis for the forward and inverse kinematics, and make it possible to understand the interface behavior. Three geometry equations relate the joint variables to the handle variables and are found using [2] as a guide. To derive the kinematics of the interface, three vector loop equations are written relating the joint variables to the handle variables:

$$(x_H - e \cos(\phi + \alpha))^2 + (y_H - e \sin(\phi + \alpha))^2 - d_1^2 = 0 \quad (2-1)$$

$$(x_H - e \cos(\phi + \alpha) - x_Q + h_2 \cos(\phi))^2 + (y_H - e \sin(\phi + \alpha) - y_Q + h_2 \sin(\phi))^2 - d_2^2 = 0 \quad (2-2)$$

$$(x_H - e \cos(\phi + \alpha) - x_R + h_1 \cos(\phi + \beta))^2 + (y_H - e \sin(\phi + \alpha) - y_R + h_1 \sin(\phi + \beta))^2 - d_3^2 = 0 \quad (2-3)$$

These three equations are used to find the inverse and forward kinematics, as discussed in subsequent sections.

2.3.2 Inverse Kinematics

The inverse kinematic equations allow calculation of the joint variables d_1 , d_2 , and d_3 given the handle variables x_H , y_H , and ϕ :

$$d_1 = g_1(x_H, y_H, \phi) \quad (2-4)$$

$$d_2 = g_2(x_H, y_H, \phi) \quad (2-5)$$

$$d_3 = g_3(x_H, y_H, \phi) \quad (2-6)$$

These equations are required for position control applications; the desired handle location is used to determine corresponding desired joint variables, which are actively controlled.

As mentioned previously the inverse kinematics for a parallel device are straightforward. The inverse kinematic equations are derived for this manipulator using equations (2-1), (2-2), and (2-3). The results are given by

$$d_1 = \sqrt{(x_H - e \cos(\phi + \alpha))^2 + (y_H - e \sin(\phi + \alpha))^2} \quad (2-7)$$

$$d_2 = \sqrt{(x_H - e \cos(\phi + \alpha) - x_Q + h_2 \cos(\phi))^2 + (y_H - e \sin(\phi + \alpha) - y_Q + h_2 \sin(\phi))^2} \quad (2-8)$$

$$d_3 = \sqrt{(x_H - e \cos(\phi + \alpha) - x_R + h_1 \cos(\phi + \alpha))^2 + (y_H - e \sin(\phi + \alpha) - y_R + h_1 \sin(\phi + \alpha))^2} \quad (2-9)$$

Using these equations it is possible to find the joint lengths from any set of handle coordinates.

2.3.3 Forward Kinematics

The forward or direct kinematic equations represent a significant challenge in the analysis of parallel manipulators. Multiple solutions often exist for a given input, and these solutions typically cannot be obtained analytically. In haptic simulations, the forward kinematic equations allow calculation of the handle location and orientation \mathbf{x} , which is comprised of x_H , y_H , and ϕ , from the measured joint lengths d_1 , d_2 , and d_3 :

$$x_H = f_x(d_1, d_2, d_3) \quad (2-10)$$

$$y_H = f_y(d_1, d_2, d_3) \quad (2-11)$$

$$\phi = f_\phi(d_1, d_2, d_3) \quad (2-12)$$

The solution of the forward kinematics is obtained using a combination of analytical and numerical methods, and proceeds as follows. Let L represent (2-1), M represent (2-2), and N represent (2-3). Subtracting M and N from L to eliminate squared terms yields

$$\begin{aligned} L - M = & -d_1^2 + d_2^2 + (-\text{ecos}(\alpha + \phi) + x_H)^2 \\ & - (-\text{ecos}(\alpha + \phi) + \cos(\phi)h_2 + x_H - x_Q)^2 \\ & + (-\text{esin}(\alpha + \phi) + y_H)^2 - (-\text{esin}(\alpha + \phi) + \sin(\phi)h_2 + y_H)^2 \end{aligned} \quad (2-13)$$

$$\begin{aligned} L - N = & -d_1^2 + d_3^2 + (-\text{ecos}(\alpha + \phi) + x_H)^2 - (-\text{ecos}(\alpha + \phi) + \cos(\beta + \phi)h_1 + \\ & x_H - x_R)^2 + (-\text{esin}(\alpha + \phi) + y_H)^2 - (-\text{esin}(\alpha + \phi) + \sin(\beta + \phi)h_1 + y_H - y_R)^2 \end{aligned} \quad (2-14)$$

Equations (2-13) and (2-14) may be used to find x_H and y_H in terms of ϕ . Substituting (2-15) and (2-16) into (2-1) yields an equation that can be used to solve for the handle variable ϕ given the joint variables d_1 , d_2 , and d_3 . Due to its size this equation is shown in the Appendix as equation (24). Once ϕ is obtained from this equation it is entered back into equations (2-15) and (2-16) to find the remaining two handle variables x_H and y_H . The set of handle variables \mathbf{x} are

thereby solved from the measured joint variables, which is used in haptic simulations to determine the location and orientation of the user's hand.

$$\begin{aligned}
x_H = & -\frac{1}{-2\cos(\phi)h_2 + 2x_Q} (-d_1^2 + d_2^2 + 2e\cos(\phi)\cos(\alpha + \phi)h_2 \\
& + 2e\sin(\phi)\sin(\alpha + \phi)h_2 - \cos(\phi)^2h_2^2 - \sin(\phi)^2h_2^2 - 2e\cos(\alpha \\
& + \phi)x_Q + 2\cos(\phi)h_2x_Q - x_Q^2) - (2\sin(\phi)h_2(-2\cos(\beta \\
& + \phi)d_1^2h_1 + 2\cos(\beta + \phi)d_2^2h_1 + 2\cos(\phi)d_1^2h_2 - 2\cos(\phi)d_3^2h_2 \\
& + 4e\cos(\beta + \phi)\sin(\phi)\sin(\alpha + \phi)h_1h_2 - 4e\cos(\phi)\sin(\alpha \\
& + \phi)\sin(\beta + \phi)h_1h_2 + 2\cos(\phi)\cos(\beta + \phi)^2h_1^2h_2 \\
& + 2\cos(\phi)\sin(\beta + \phi)^2h_1^2h_2 - 2\cos(\phi)^2\cos(\beta + \phi)h_1h_2^2 \\
& - 2\cos(\beta + \phi)\sin(\phi)^2h_1h_2^2 - 2d_1^2x_Q + 2d_3^2x_Q + 4e\sin(\alpha \\
& + \phi)\sin(\beta + \phi)h_1x_Q - 2\cos(\beta + \phi)^2h_1^2x_Q \\
& - 2\sin(\beta + \phi)^2h_1^2x_Q + 4\cos(\phi)\cos(\beta + \phi)h_1h_2x_Q - 2\cos(\beta \\
& + \phi)h_1x_Q^2 + 2d_1^2x_R - 2d_2^2x_R - 4e\sin(\phi)\sin(\alpha + \phi)h_2x_R \\
& - 4\cos(\phi)\cos(\beta + \phi)h_1h_2x_R + 2\cos(\phi)^2h_2^2x_R + 2\sin(\phi)^2h_2^2x_R \\
& + 4\cos(\beta + \phi)h_1x_Qx_R - 4\cos(\phi)h_2x_Qx_R + 2x_Q^2x_R \\
& + 2\cos(\phi)h_2x_R^2 - 2x_Qx_R^2 + 4e\cos(\phi)\sin(\alpha + \phi)h_2y_R \\
& - 4\cos(\phi)\sin(\beta + \phi)h_1h_2y_R - 4e\sin(\alpha + \phi)x_Qy_R + 4\sin(\beta \\
& + \phi)h_1x_Qy_R + 2\cos(\phi)h_2y_R^2 - 2x_Qy_R^2)/((-2\cos(\phi)h_2 \\
& + 2x_Q)(-4\cos(\beta + \phi)\sin(\phi)h_1h_2 + 4\cos(\phi)\sin(\beta + \phi)h_1h_2 \\
& - 4\sin(\beta + \phi)h_1x_Q + 4\sin(\phi)h_2x_R - 4\cos(\phi)h_2y_R + 4x_Qy_R))
\end{aligned} \tag{2-15}$$

This information is used to calculate the feedback forces and torques to apply to the user's hand, based on the interactions of the virtual hand with the virtual environment.

Due to the complexity of equation (24) *Mathematica* is used to determine a numerical solution for ϕ for a given set of joint variables. The specific solving function employed,

FindRoot, requires an initial guess for ϕ . Multiple solutions are possible for a given input \mathbf{q} , with the resulting solution being dependent on the initial guess.

$$\begin{aligned}
y_H = & -(-2\cos(\beta + \phi)d_1^2h_1 + 2\cos(\beta + \phi)d_2^2h_1 + 2\cos(\phi)d_1^2h_2 \\
& - 2\cos(\phi)d_3^2h_2 + 4\cos(\beta + \phi)\sin(\phi)\sin(\alpha + \phi)h_1h_2 \\
& - 4\cos(\phi)\sin(\alpha + \phi)\sin(\beta + \phi)h_1h_2 \\
& + 2\cos(\phi)\cos(\beta + \phi)^2h_1^2h_2 + 2\cos(\phi)\sin(\beta + \phi)^2h_1^2h_2 \\
& - 2\cos(\phi)^2\cos(\beta + \phi)h_1h_2^2 - 2\cos(\beta + \phi)\sin(\phi)^2h_1h_2^2 \\
& - 2d_1^2x_Q + 2d_3^2x_Q + 4\sin(\alpha + \phi)\sin(\beta + \phi)h_1x_Q \\
& - 2\cos(\beta + \phi)^2h_1^2x_Q - 2\sin(\beta + \phi)^2h_1^2x_Q + 4\cos(\phi)\cos(\beta \\
& + \phi)h_1h_2x_Q - 2\cos(\beta + \phi)h_1x_Q^2 + 2d_1^2x_R - 2d_2^2x_R \\
& - 4\sin(\phi)\sin(\alpha + \phi)h_2x_R - 4\cos(\phi)\cos(\beta + \phi)h_1h_2x_R \\
& + 2\cos(\phi)^2h_2^2x_R + 2\sin(\phi)^2h_2^2x_R + 4\cos(\beta + \phi)h_1x_Qx_R \\
& - 4\cos(\phi)h_2x_Qx_R + 2x_Q^2x_R + 2\cos(\phi)h_2x_R^2 - 2x_Qx_R^2 \\
& + 4\cos(\phi)\sin(\alpha + \phi)h_2y_R - 4\cos(\phi)\sin(\beta + \phi)h_1h_2y_R \\
& - 4\sin(\alpha + \phi)x_Qy_R + 4\sin(\beta + \phi)h_1x_Qy_R + 2\cos(\phi)h_2y_R^2 \\
& - 2x_Qy_R^2)/(-4\cos(\beta + \phi)\sin(\phi)h_1h_2 + 4\cos(\phi)\sin(\beta \\
& + \phi)h_1h_2 - 4\sin(\beta + \phi)h_1x_Q + 4\sin(\phi)h_2x_R - 4\cos(\phi)h_2y_R \\
& + 4x_Qy_R)
\end{aligned} \tag{2-16}$$

2.4 Velocity Kinematics

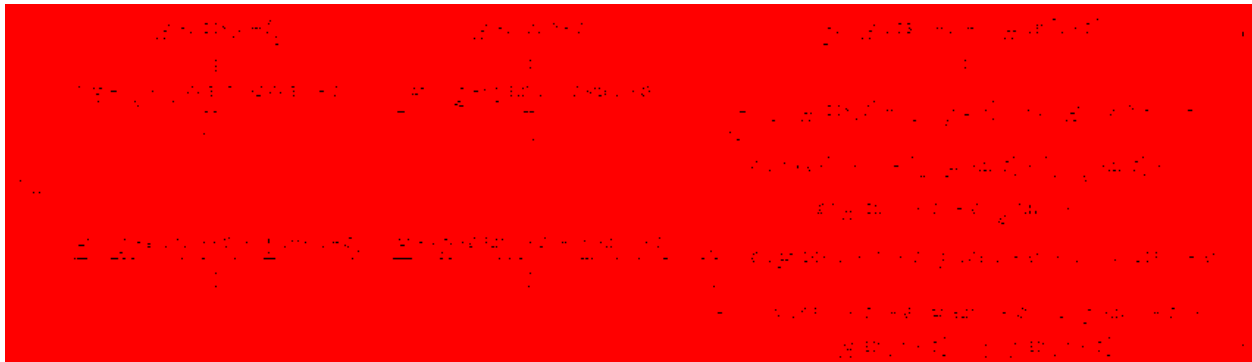
The forward kinematic equations allow a user to send position and orientation input signals through the interface. The velocity relationship between the handle and the joints is understood with the Jacobian of the system. Additionally, the Jacobian describes the static force and torque relationships of the system. The Jacobian is also critical for the determination of the manipulability of the end-effector.

2.4.1 Jacobian

The velocity of the joint variables is related to the handle variables via the Jacobian, or first derivative of the geometry equations. For parallel manipulators, this relationship is given as

$$\dot{\mathbf{q}} = J\dot{\mathbf{x}} \quad (2-17)$$

where $\dot{\mathbf{q}}$ is the joint space velocity vector, $\dot{\mathbf{x}}$ is the handle velocity vector, and J is the Jacobian of the manipulator [2]. Note that this is the inverse of the definition typically employed for serial manipulators. Equation (2-17) may be used to solve for the handle velocities given the joint velocities, or vice versa. The Jacobian is a central part of this project. It maps the coordinate space, \mathbf{x} into the joint space, \mathbf{q} . The Jacobian is used to find the velocity kinematics and is also used to measure manipulability. For this 3-RPR manipulator the Jacobian was found analytically by taking the first derivative of the kinematic equations, and is given by


$$J = \begin{bmatrix} \frac{\partial x_1}{\partial \theta_1} & \frac{\partial x_1}{\partial \theta_2} & \frac{\partial x_1}{\partial \theta_3} & \frac{\partial x_2}{\partial \theta_1} & \frac{\partial x_2}{\partial \theta_2} & \frac{\partial x_2}{\partial \theta_3} \\ \frac{\partial y_1}{\partial \theta_1} & \frac{\partial y_1}{\partial \theta_2} & \frac{\partial y_1}{\partial \theta_3} & \frac{\partial y_2}{\partial \theta_1} & \frac{\partial y_2}{\partial \theta_2} & \frac{\partial y_2}{\partial \theta_3} \\ \frac{\partial z_1}{\partial \theta_1} & \frac{\partial z_1}{\partial \theta_2} & \frac{\partial z_1}{\partial \theta_3} & \frac{\partial z_2}{\partial \theta_1} & \frac{\partial z_2}{\partial \theta_2} & \frac{\partial z_2}{\partial \theta_3} \end{bmatrix}$$

After developing the Jacobian, an alternate method was used to verify its correctness. A numerical approximation using a centered finite-difference formula was used to determine both the velocity of the handle variables and the velocity of the joint variables, $\dot{\mathbf{x}}$ and $\dot{\mathbf{q}}$. Both methods (Jacobian and numerical differentiation) yielded the same velocity results, instilling confidence that the analytically derived model is correct.

2.4.2 Statics

As stated previously the Jacobian relates changes in the coordinate space to the joint space. In addition to relating velocities, the Jacobian describes the static force and torque relationships of the haptic interface. The handle forces/torques are found in terms of the actuated joint torques/forces, and vice versa [2]. This relationship for parallel manipulators is given by [2]

$$\mathbf{F} = \mathbf{J}^T \boldsymbol{\tau} \quad (2-18)$$

where, \mathbf{F} represents the vector of end-effector output force and torque, $\boldsymbol{\tau}$ represents the vector of actuated joint torques or forces, and \mathbf{J} represents the Jacobian. Again, this is the inverse of the definition typically employed for serial manipulators. Given the handle force and torque \mathbf{F} , (2-18) can be used to find the joint forces $\boldsymbol{\tau}$, and vice versa. This is especially important in haptic simulations, in which it is necessary to calculate the forces that the actuators must exert to apply the desired forces and torques at the handle to a user. In general, \mathbf{F} (the force that the user should feel) is calculated in the haptic simulation based on interactions in the virtual world. The haptic interface cannot apply \mathbf{F} directly to the user's hand via the handle. Instead, the joint forces $\boldsymbol{\tau}$ must be calculated and applied to give the desired \mathbf{F} at the handle. Equation (2-18) enables the computer to solve for the joint forces that yield the desired handle forces and torques.

2.5 Singularities and Manipulability

As stated previously, the objective of this work is to optimize the design of the planar haptic interface based on manipulability and singularity avoidance. Singularities in a system

occur when there is a loss of one or more degrees of freedom. The goal is to design an interface that will not allow a handle to encounter singularities within the desired workspace.

A method to determine if a singularity exists is to take the determinant of the Jacobian at a given handle configuration [2] [31]. This definition makes sense considering equation (2-18). The joint forces, τ can only be mapped into the handle output force, F when the Jacobian is invertible. If the determinant of the Jacobian is zero then the Jacobian is no longer invertible and the joint forces cannot translate into handle forces. The handle configurations that yield a determinant of the Jacobian equal to zero are locations in which singularities exist. As stated in [32], “At certain manipulator configurations, the Jacobian matrix may lose its full rank (i.e., there is a reduction of the number of linearly independent rows or columns). Hence as the manipulator approaches these configurations, the Jacobian matrix becomes ill conditioned and may not be invertible.” It follows that as an end-effector moves away from ill-conditioned and singular configurations the joint forces map into the handle forces providing the desired output to a user.

The determinant of the Jacobian yields a single scalar value. This scalar value helps the designer determine valid constraints and designs for the manipulator. Ultimately this value is used to optimize a workspace through singularity avoidance and manipulability valuation. It is the designer's task to find the optimal placement of the bases P , Q , and R as seen in Figure 2-1 to select the best singularity-free workspace.

Manipulability (ω) is a measure of the ability of the interface to exert forces and torque uniformly in all directions on a user. As just discussed the determinant of the Jacobian is a measure of the ability of an interface to exert forces and torques uniformly in all directions on a user; thus, for the purposes of this work, the manipulability is shown in equation (2-19).

To find the level of manipulability of the end effector it is required to take the determinant of the Jacobian matrix at discrete handle positions. As the handle position nears a singularity, its manipulability decreases. If the determinant is zero, then the manipulability is zero and the interface is in a singular configuration. If the Jacobian is ill-conditioned, then the manipulability is small (but not zero), indicating that the interface can exert forces and torques in that configuration, but at a reduced level. The areas of zero, low, and high manipulability of an end-effector for a given design can be mapped by altering the handle position across a region at discrete points and measuring the manipulability. This process is used in a subsequent chapter to value a design.

$$\omega = \text{Det}[J] \quad (2-19)$$

To better understand manipulability we first look at an example. A simple two-bar serial manipulator is depicted in Figure 2-2.

A computer algorithm was created in Mathematica to aid in visualization of the manipulability of the handle H. In the first configuration, shown in Figure 2-3 (a), manipulability is at a maximum and the handle can exert force uniformly in all directions. In the second configuration, shown in Figure 2-3 (b), manipulability is zero, indicating that the manipulator has encountered a singularity. The reason for the manipulability loss is simple; the end effector has lost a degree of freedom in the radial direction. Note that the angle of the longer bar did not have any effect on the manipulability measure.

The 3-dimensional plot in Figure 2-4 (a), shows that the value of θ_1 has no effect on the manipulability of the system. As the shorter bar of length a_2 moves through different angles the

manipulability measure changes from a maximum to a minimum. The maximum manipulability for this system is found when θ_2 is at $\pm 90^\circ$.

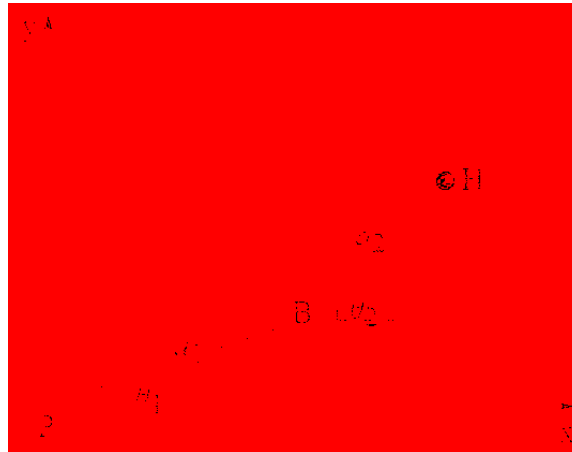


Figure 2-2: Two-bar Mechanism

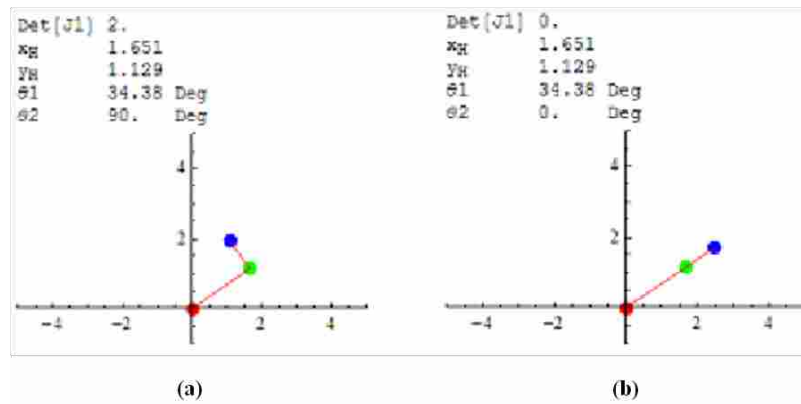


Figure 2-3: Manipulability Measure on a Simple Two-bar Mechanism

An alternate way to think of manipulability is to imagine that the two-bar mechanism just examined is the human arm. Humans naturally observe the laws of manipulability by putting their arm in a 90° angle when they write [31]. Positioned thus, it is easy for a writer to move

their hand in any direction. Once the arm is fully extended a degree of freedom is lost; it can no longer exert force directly away from the body and it is more difficult to exert force in a sideways direction. Thus configured the arm has lost its manipulability.

Now that we know that θ_1 has no effect on the manipulability measure for this system a simple 2D plot can more easily demonstrate the manipulability of the handle, as shown in Figure 2-4 (b).

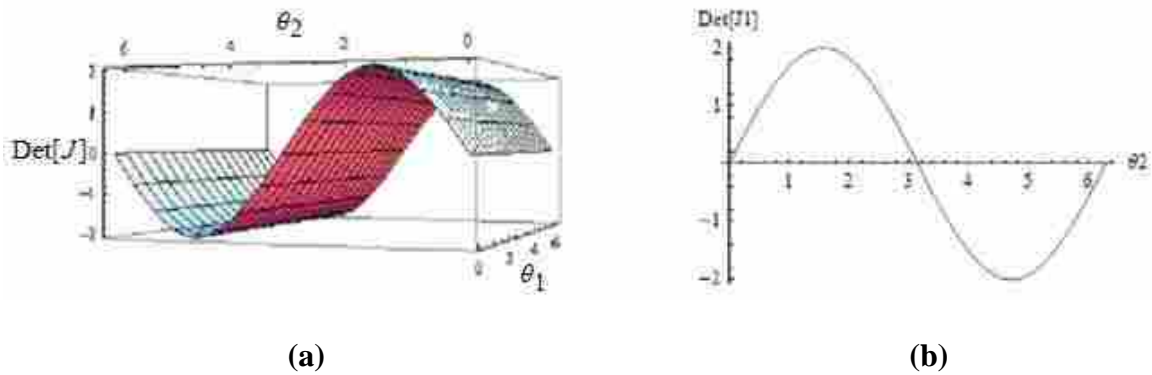


Figure 2-4: Manipulability Measure Graphs for a Two-bar Mechanism

To understand the manipulability measure for the planar parallel interface under examination in this work, a simple example with ϕ held at zero is shown Figure 2-5 (a). The optimization of the 3-RPR parallel planar design takes into account a changing ϕ , however, for this example ϕ is held constant. The 3D plot in Figure 2-5 (b) shows how the manipulability changes as the handle moves in the plane by changing x_H and y_H . The points where the $\text{Det}[J]$ is equal to zero are the singularities. In the Figure 2-5 (c) the plot is sliced at zero to more easily see the singularities in the manipulability map. Only the edge of the slice represents a singularity. All other measures of the manipulability above

and below the zero plane are determined to be acceptable workspaces; in other words they are free of singularities.

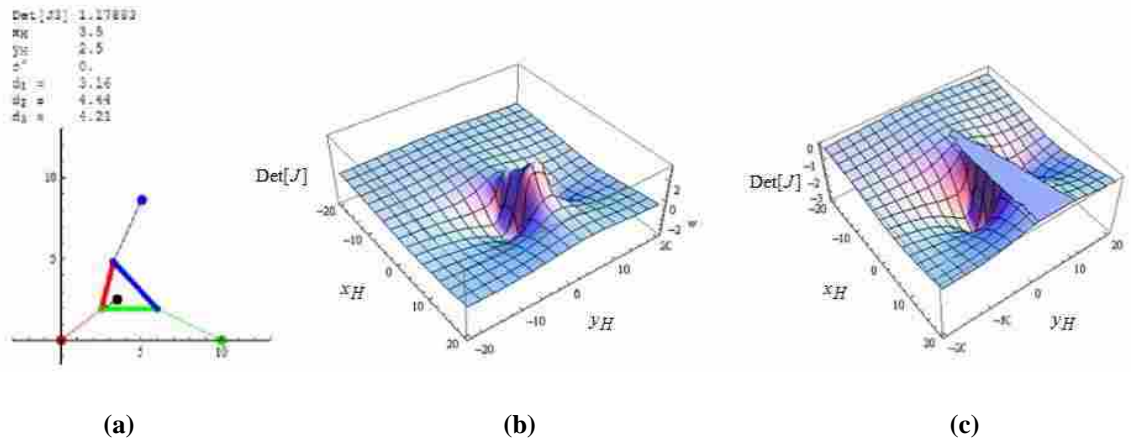


Figure 2-5: Manipulability Map With $\phi = 0$ for a Planar 3-RPR Parallel Mechanism

As in the example of a fully extended simple two bar mechanism, there are configurations in the 3-RPR manipulator where ω is equal to zero. Figure 2-6 shows a measure of the manipulability for only one location: the handle. The manipulability measure is zero at the handle location because the perfectly equilateral triangle configuration of the bases, combined with a ϕ value equal to zero, is a configuration that causes a loss of one degree of freedom: no torque can be exerted on the handle, the manipulability is zero. Note the intersecting lines at the very center of the handle. The prismatic joints can only exert force along those lines. With the angle set at 0° the handle cannot be rotated via the joints.

Contrast Figure 2-6 with Figure 2-7. Figure 2-7 has the exact same design, however, ϕ is fixed at 45° . Note that because of this change in angle of the handle the lines indicating the direction of joint forces no longer intersect. In this case the handle has been moved across the entire region and the measure of manipulability has been mapped. The heavy shaded areas of the

map indicate singularities or regions that the end-effector cannot reach due to physical constraints. The lighter regions of the plot are contour lines indicating the measure of manipulability. This comparison highlights the need to find areas of manipulability for all desired positions of the handle, including not only a translational region but a rotational range through which the handle will move.

To effectively determine the value of a configuration of bases, or in other words the value of the design, a manipulability map is required. The workspaces found from the manipulability map must be separated, valued, and compared to determine the best design of the haptic interface. This process is the topic of the next chapter.

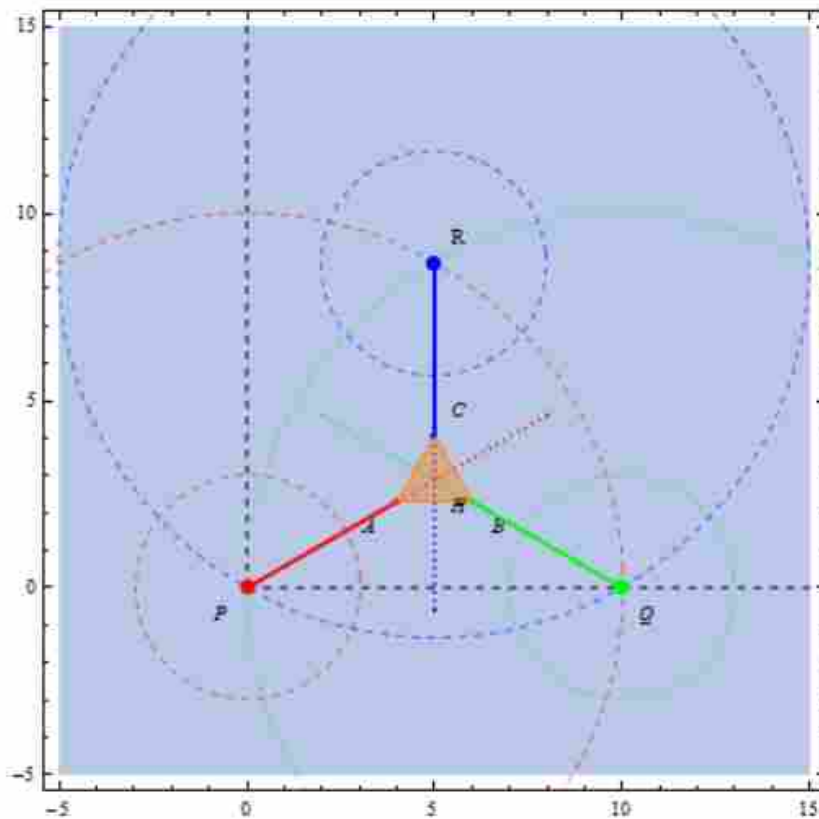


Figure 2-6: Singularity Configuration for Planar 3-RPR Parallel Mechanism

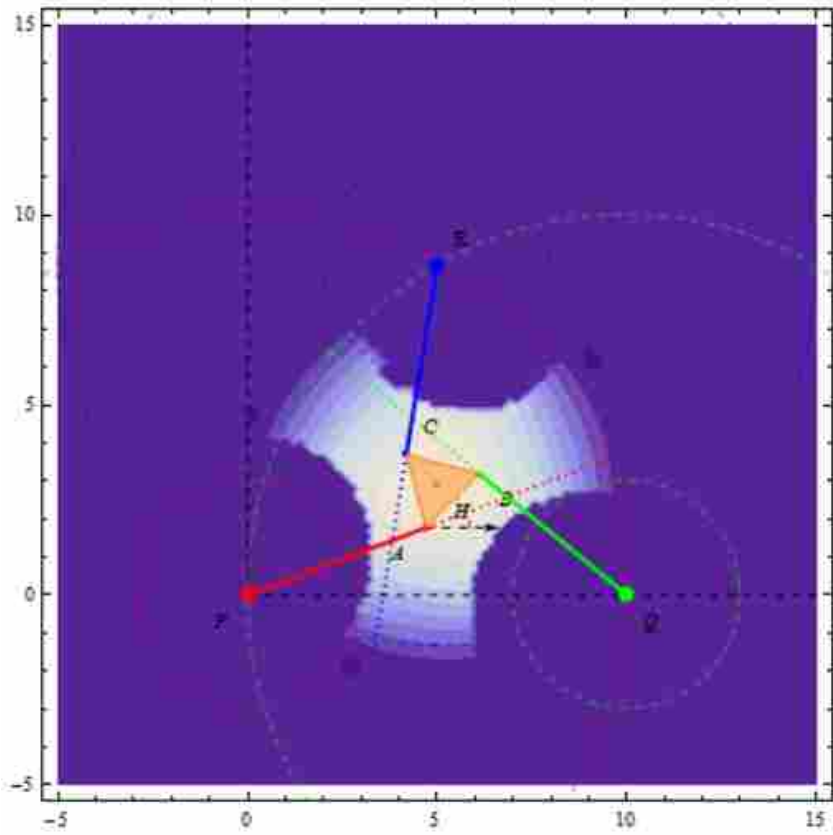


Figure 2-7: Manipulability Map of 3-RPR Manipulator With $\phi = 45^\circ$

3 OPTIMIZATION METHOD

3.1 Overview

The objective of the optimization algorithm is to find the locations of the bases, Q and R , that will yield an optimal workspace based on manipulability (including average manipulability and standard deviation of the manipulability across the workspace) and geometry (including both size and shape) of the workspace. The objective is focused on enhancing the interface for haptic use.

This chapter discusses in detail the general procedures required to perform this optimization. Designs are processed, workspaces are generated and characterized and optimization filters are used to reduce the number of workspace options from many to only a few. The designer then makes an informed decision on which design to select based on the metrics that characterize the workspace and the particular desires of the designer. The designer selects the combination of workspace geometry and manipulability that they want and the optimal design is selected. The bases that correspond to the selected design are determined and the resulting configuration is considered to be optimally designed for haptic applications.

For convenience the diagram of the 3-RPR parallel planar device is repeated in Figure 3-1. Each possible configuration of the bases must be examined and the manipulability of the handle mapped as it moves through the entire possible workspace. This is accomplished by using an algorithm to go through each unique set of base locations.

A unique configuration or location for each base Q and R is chosen. There is no need to move base P ; it only requires one location that acts as an anchor for the manipulator. Additional movement of P would only cause redundant effort with no value added. Each unique configuration of Q and R is considered a design. Once chosen, the end effector or handle is stepped through the reachable region, subject to the position kinematics of the system. At each point the manipulability is determined and stored. Once the regions are measured, the configuration of bases Q and R is perturbed and a new region specific to the new design is mapped. This process continues until all defined configurations of Q and R , at the specified resolution, have been exhausted. The processing time for this operation depends on the selected resolution or number of Q and R base locations.

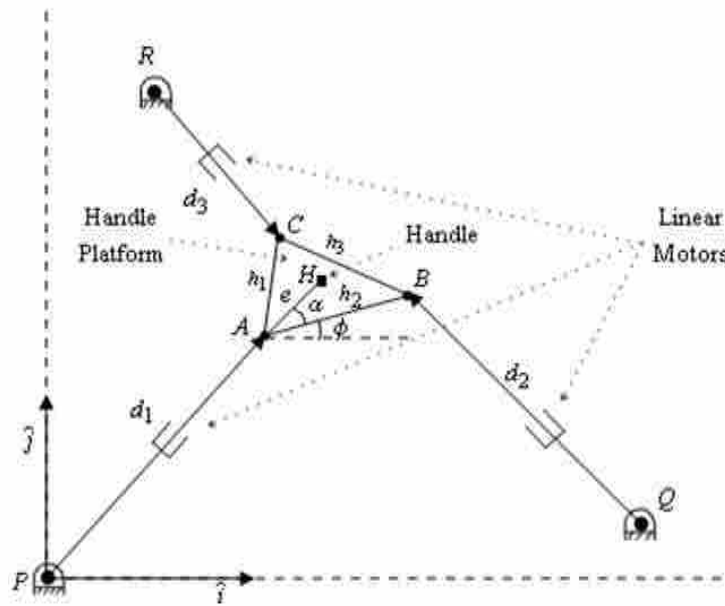


Figure 3-1: Planar 3-RPR Parallel Mechanism

The mapped regions will often contain more than one workspace. Locations in the region containing singularities and measures of manipulability near zero are unusable and cannot be

considered part of any workspace. These singularities cut through the regions, leaving distinct regions of non-zero manipulability. Whether positive or negative, these non-zero regions represent potentially usable workspaces.

The workspaces are identified, separated, and characterized in terms of area, compactness, mean manipulability, and standard deviation of manipulability. Once characterized the workspaces are placed in a candidate workspaces set and the process is repeated: a new design is selected and its workspaces are characterized. After all designs have been characterized and their workspaces placed in the candidate workspaces set it is necessary to use optimization techniques to select the best workspace and corresponding design.

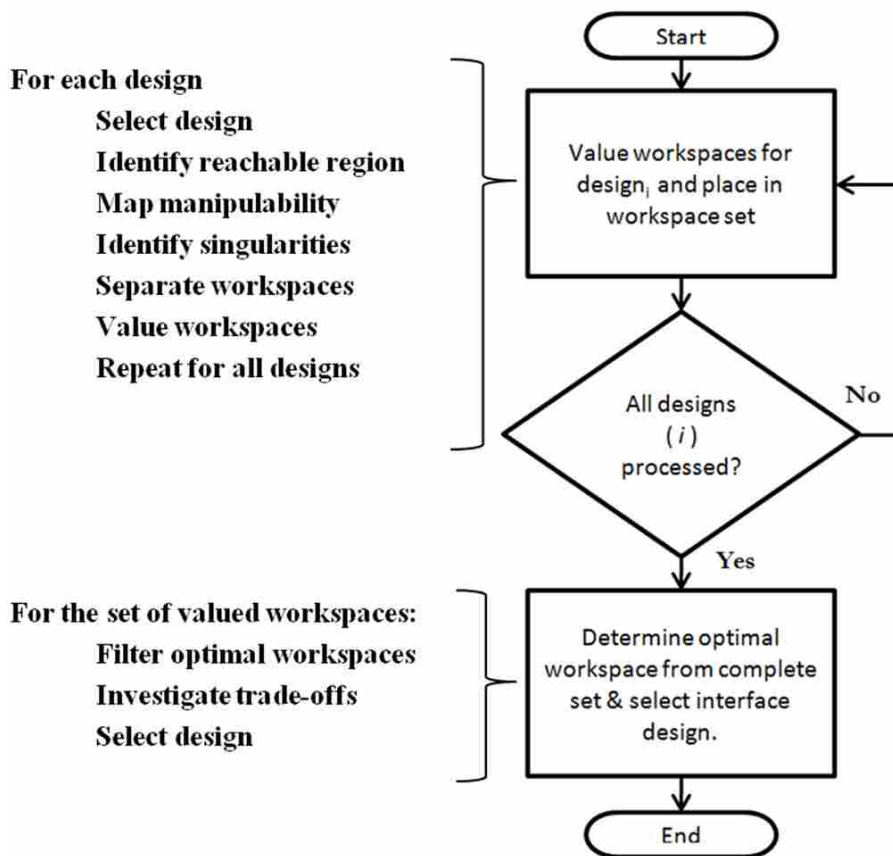


Figure 3-2: General Optimization Method Flow Chart

The designs are filtered using a series of Pareto filters designed to handle multi-objective optimization. After the Pareto filters have reduced the number of designs to a desired size, the designer examines each of the top candidates and selects the one that represents their particular interest. A detailed description of each of the basic steps involved in this process follows. Before proceeding to this discussion, a flow chart of the general method just presented is shown in Figure 3-2. The intention is to give a basic, overall idea of the approach. Each of the steps is discussed in detail in the subsequent sections. A formal optimization statement of the general method is given following a detailed description of the method used in this thesis.

3.2 Selection of Base Configurations

A design in this context is simply a reconfiguration of the bases. Each adjustment of the design can result in a different workspace or set of workspaces. The number of designs that can be checked is limited by the geometry of the manipulator. Only designs that can be reached by the bases can be considered. Additionally, the region that is reachable has locations at which the bases may be placed. As the location possibilities are infinite, the designer is required to choose a resolution greater than zero over which to search: total search region divided by resolution. This technique yields a finite number of locations at which bases are placed. This discretization of the search region is necessary to place the bases. The same method is employed to create a search area for the handle placements as the manipulability map is created. The resolution should be a sufficient size to locate singularities and discover the usable workspace in the search region.

A simple algorithm is coded to run through the designer's selection of designs at the specified resolution, but first the bases must be selected and the resolution set. The following describes this process for each of the bases.

3.2.1 Selection of Base P

Base P acts as an anchor point and does not move. It is considered to be at a Cartesian coordinate of $(0, 0)$ in the plane, as shown in Figure 3-3. As it is only a point, the search resolution is irrelevant.

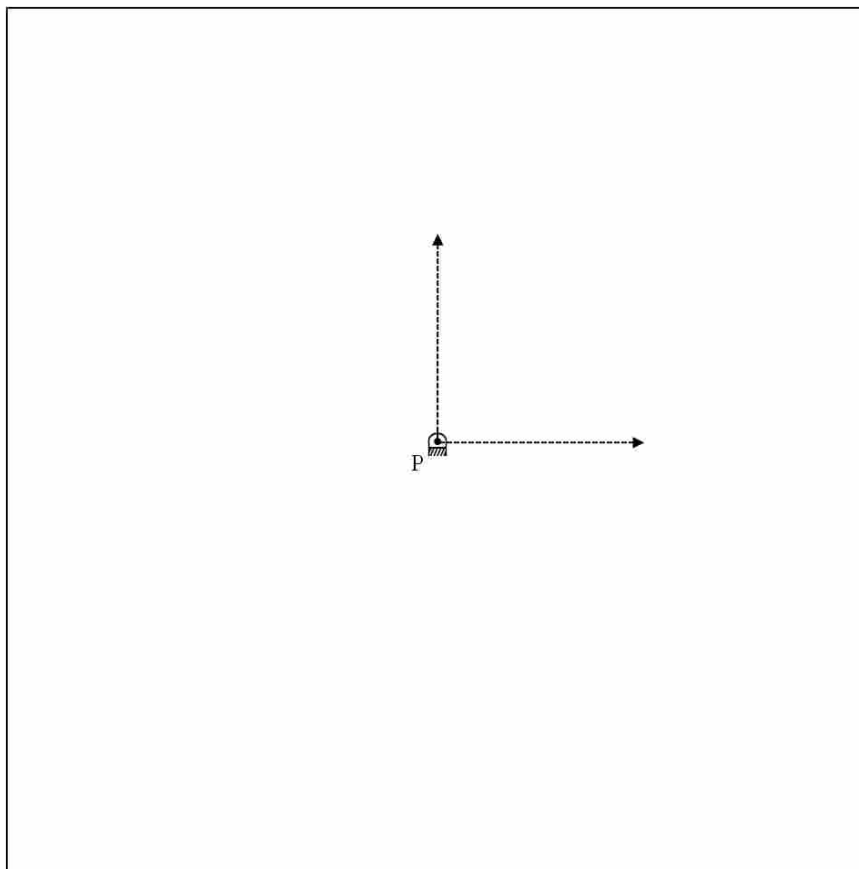


Figure 3-3: Placement of Base P

3.2.2 Search Limits

With Base P established, the maximum searchable region becomes clear. The furthest point Base Q or R may be placed from P is $2d_{\max}+h_{\max}$, where d_{\max} is the maximum extension of each motor and h_{\max} is the maximum of h_1 or h_2 . The placement of the next base then falls inside a circle of diameter $2(2d_{\max}+h_{\max})$, as shown in Figure 3-4.

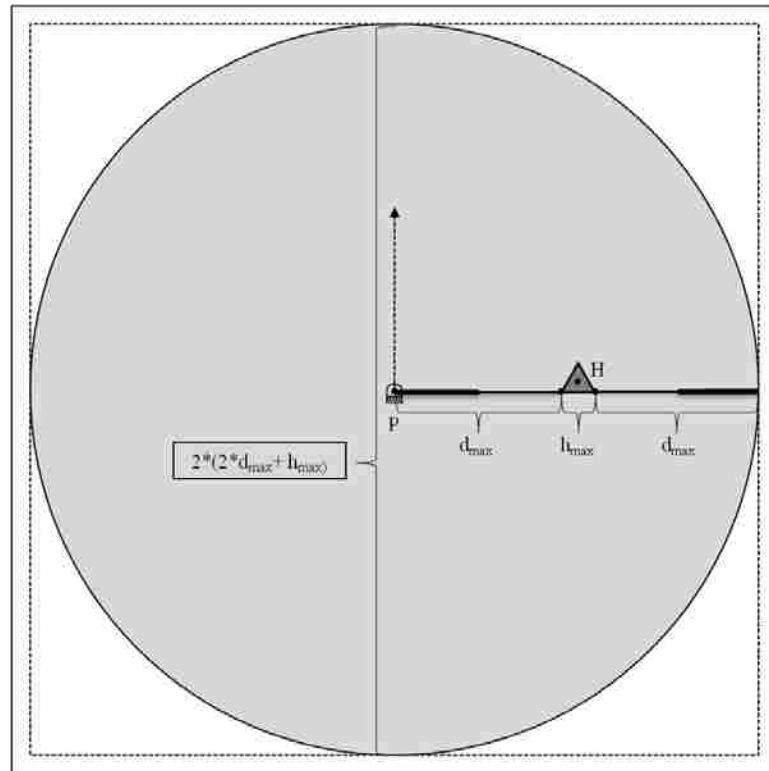


Figure 3-4: Outer Constraint of Second Base Placement

3.2.3 Selection of Base Q

Base Q is subject to the radial constraint stated in the previous section. Potential locations of Q can be limited to the x -axis without any loss of generality, since placement of Q

off of the x -axis is equivalent to simply creating a new frame rotated such that the new x -axis is pointing toward Q . As shown in Figure 3-5, Q may be placed anywhere on the x -axis between the origin and the outer extent of the radial constraint illustrated in Figure 3-4. The number of Q base locations to be tested along the x -axis is entered by the designer in terms of a $Q_{\text{Resolution}}$.

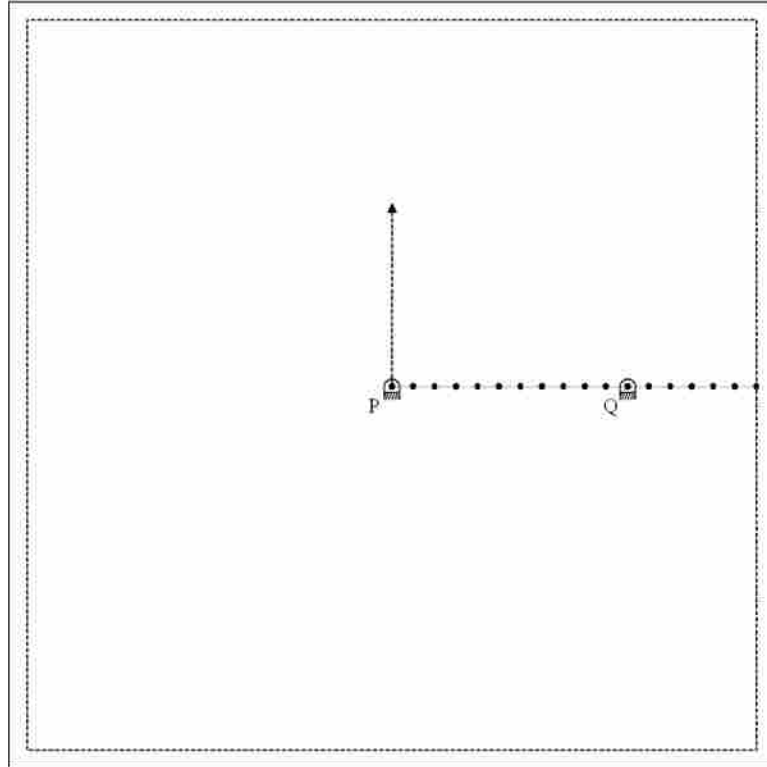


Figure 3-5: Placement of Base Q

3.2.4 Selection of Base R

The maximum distance base R can be placed from base P is $d_{1max}+h_1+d_{3max}$, letting ϕ adjust so that it does not constrain $d_{1max}+h_1+d_{3max}$ from extending in a straight line away from base P . Unlike base Q , base R is not constrained to the x -axis but is placed anywhere within range of the radial constraint. Similar to the $Q_{\text{Resolution}}$ a designer decides on the number of base

locations by setting the $R_{\text{Resolution}}$. For each selected location of base Q there is a new search region for base R . Although in practice R can only be placed within the radial constraint, practical considerations make it simpler to implement a square search grid. As each candidate location of R is examined, those that lie outside of the radial constraint are discarded. Figure 3-6 illustrates the placement of the three base points and the square search grid in which R was placed.

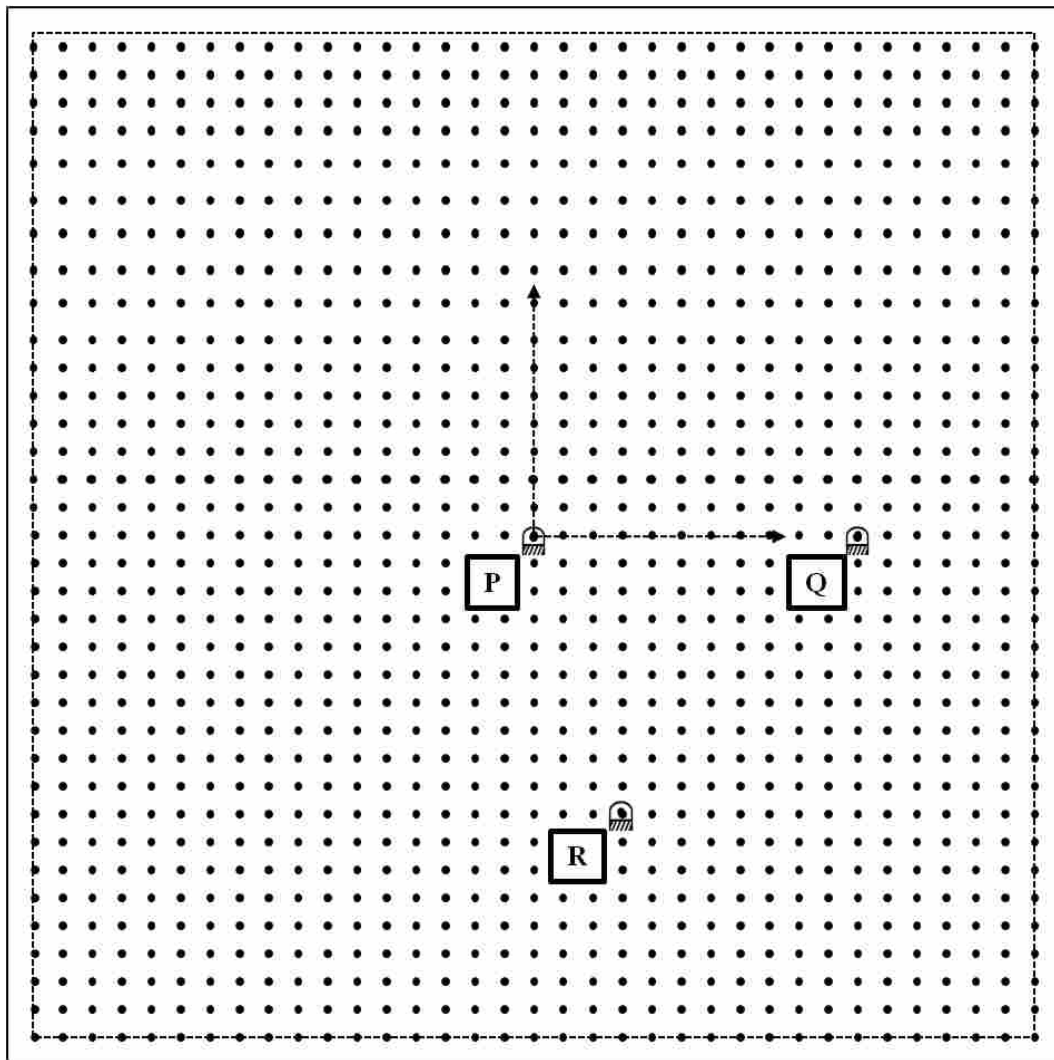


Figure 3-6: Placement of Base R

3.2.5 Total Search Region

With the bases set, a design has been selected. Prior to placing additional constraints the handle, represented by H , can be moved anywhere in the region defined for R (see Figure 3-7). The algorithm allows the handle to move over a square region, although handle locations outside its radial constraint are not considered.

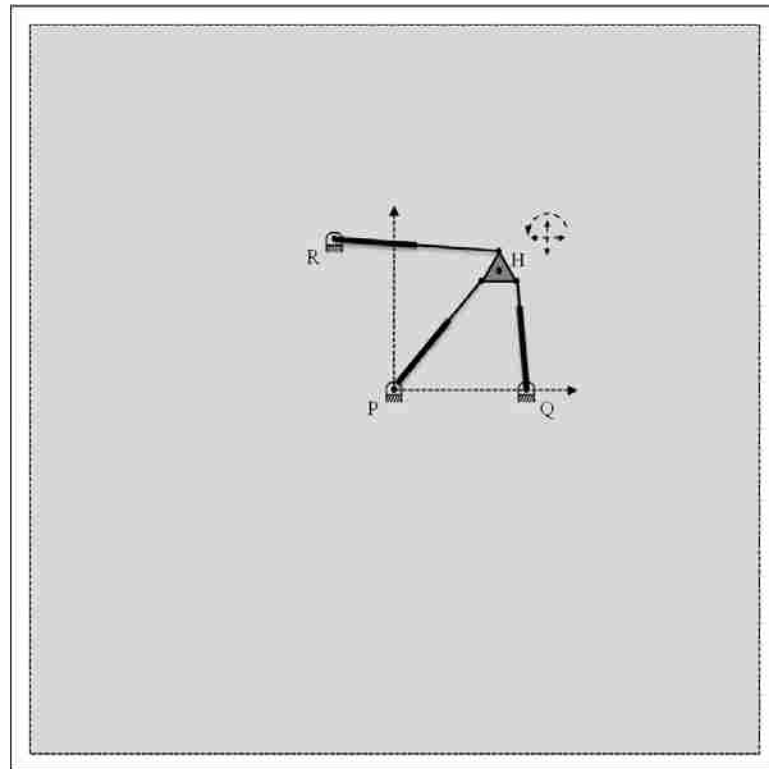


Figure 3-7: Movement of Handle, H

When a constraint is violated a zero is placed in the manipulability map just as if there were a singularity at that point. A resolution for the placement of H is also selected by the designer. The handle H is then stepped through all locations defined by the resolution and a measure of manipulability is taken at each handle position that has not violated the physical

reach constraints of the manipulator. Physical constraints are checked before measuring manipulability at each point to reduce computation time. Additionally, care should be taken to choose a sufficient sample size without overdoing it, causing undue processing time costs.

3.3 Mapping Manipulability

Once a design is selected a map of manipulability can be created. To create this map the handle is moved through the search region and the measure of manipulability is recorded at each handle location. Depending on the location of the bases, there are regions the handle cannot be placed due to its physical constraints. Before manipulability is checked a simple go, no-go check is performed to see if any constraints are violated. If a handle cannot reach a point there is no value gained from checking the manipulability. The following constraints are examined.

3.3.1 Constraints

The first step is to choose a handle configuration within a range determined using minimum and maximum lengths of the linear motors. The choice of x_A and y_A must fall outside an inner circle created by length d_{min} and within a ring of outer radius d_{max} both centered around base P , as shown in Figure 3-8 and defined as:

$$d_{min} \leq d_1 \leq d_{max} \quad (2-20)$$

The next step selects a ϕ , completing the three inputs that will for the simple case remain fixed, x_A , y_A , ϕ . The range of possible values of ϕ is based on the angle that a typical human wrist will rotate from side to side. A standard computer mouse is useful to demonstrate this constraint. When an operator is using a computer mouse there is no need to turn the mouse

completely around an imaginary z -axis coming out of the plane. Instead a mouse is fully functional within an angle to the left or to the right. Thus, a ϕ will be chosen such that:

$$\phi_{min} \leq \phi \leq \phi_{max} \quad (2-21)$$

Figures 3-9 and 3-10 assist in understanding this constraint. In Figure 3-9, $\phi = 0$, and Figure 3-10 shows the constraints shift as ϕ changes to 90° .

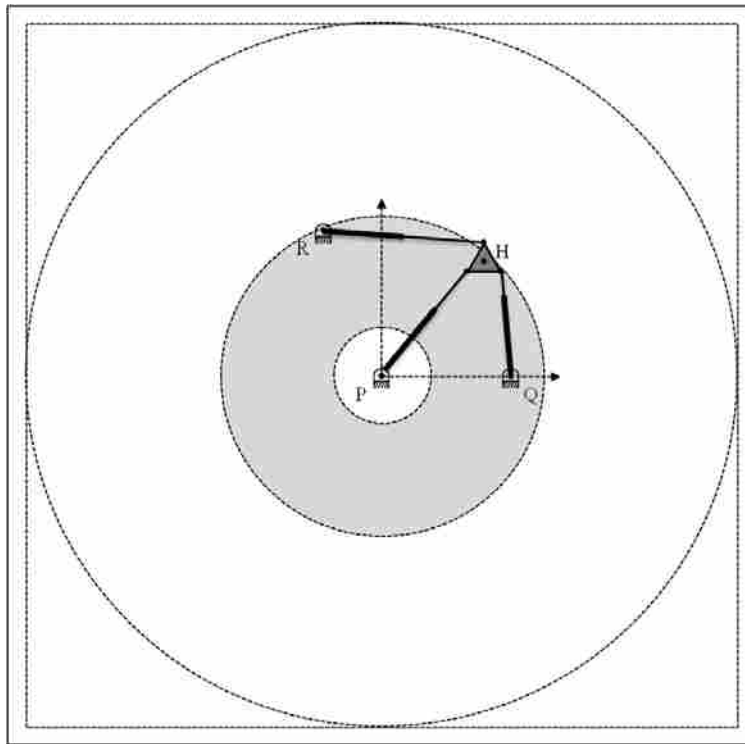


Figure 3-8: Interior Joint Length Constraints

With values for all of the following variables, x_Q , x_R , y_R , x_A , y_A , and ϕ , the measure of manipulability, ω is found. Before placing this in the map, the algorithm will try several values of ϕ from ϕ_{min} to ϕ_{max} , sampling the measure of manipulability at each increment.

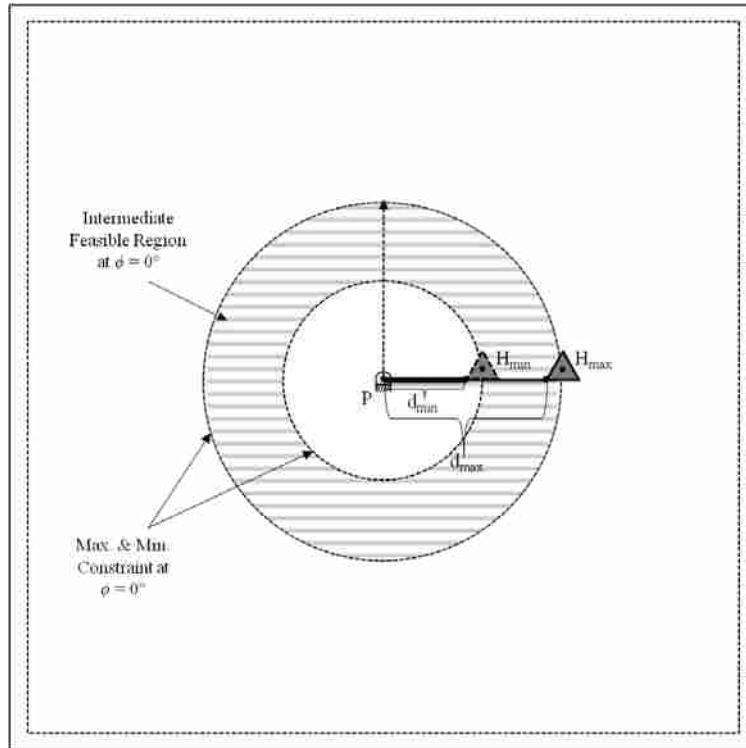


Figure 3-9: ϕ Constraints, $\phi = 0^\circ$

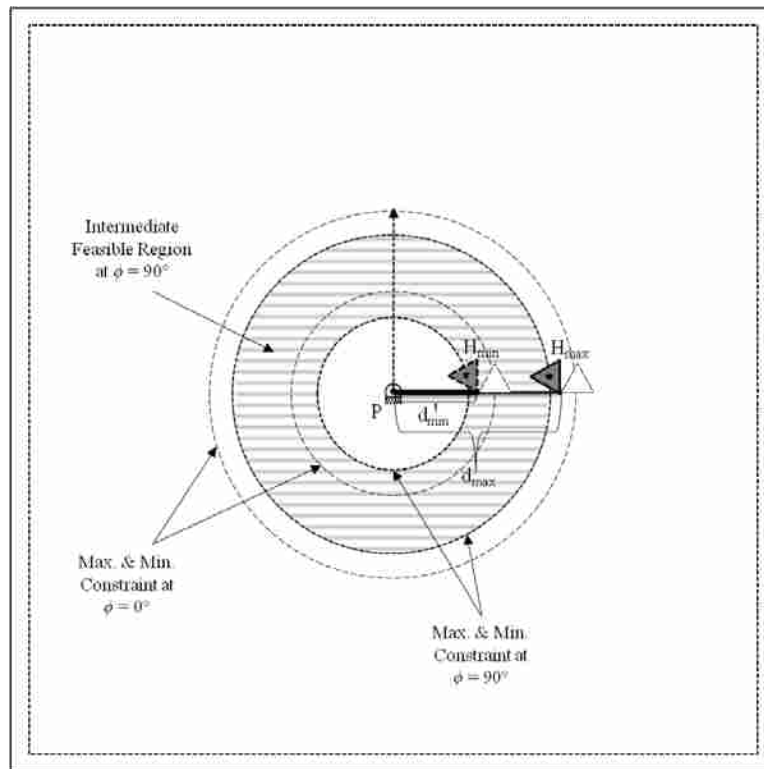


Figure 3-10: ϕ Constraints, $\phi = 90^\circ$

Only after the entire range of ϕ is sampled at the designer's choice of $\phi_{\text{Resolution}}$ will an average value of manipulability be taken and placed in the manipulability map for that specific handle location. Note that if a constraint is violated as each ϕ in the ϕ_{Range} is tested the location is considered unreachable and is shown on the manipulability map as zero. As a user moves the handle through the range of ϕ no singularities are tolerated.

For the given configuration defined by x_H , y_H , and ϕ , the problem is to find the optimal placements of the design variables x_Q , x_R , and y_R . These design variables must also follow a similar constraint used to determine x_A and y_A .

In addition to the upper and lower constraints placed on the possible location placements of bases Q and R there are some constraints imposed simply because of the position kinematics. The handle points x_B and x_C must be found within a ring of outer radius d_{max} and outside inner radius d_{min} . The center of each circle is found at Q and R just as the center of the constraint circle for x_A and y_A is found around P . This can be stated as:

$$d_{\text{min}} \leq d_2 \leq d_{\text{max}} \quad (2-22)$$

$$d_{\text{min}} \leq d_3 \leq d_{\text{max}} \quad (2-23)$$

If any of these constraints are violated it is considered an invalid point and a value of zero will be recorded on the manipulability map. To better understand these constraints, assume a fixed angle $\phi = 0^\circ$ and examine the diagram in Figure 3-11.

Assuming that every placement of the handle does not violate a constraint mentioned in the previous section, some region is left that needs its manipulability measured. As an example, assume that the region in gray is the space left after all constraints have been satisfied, as shown in Figure 3-12.

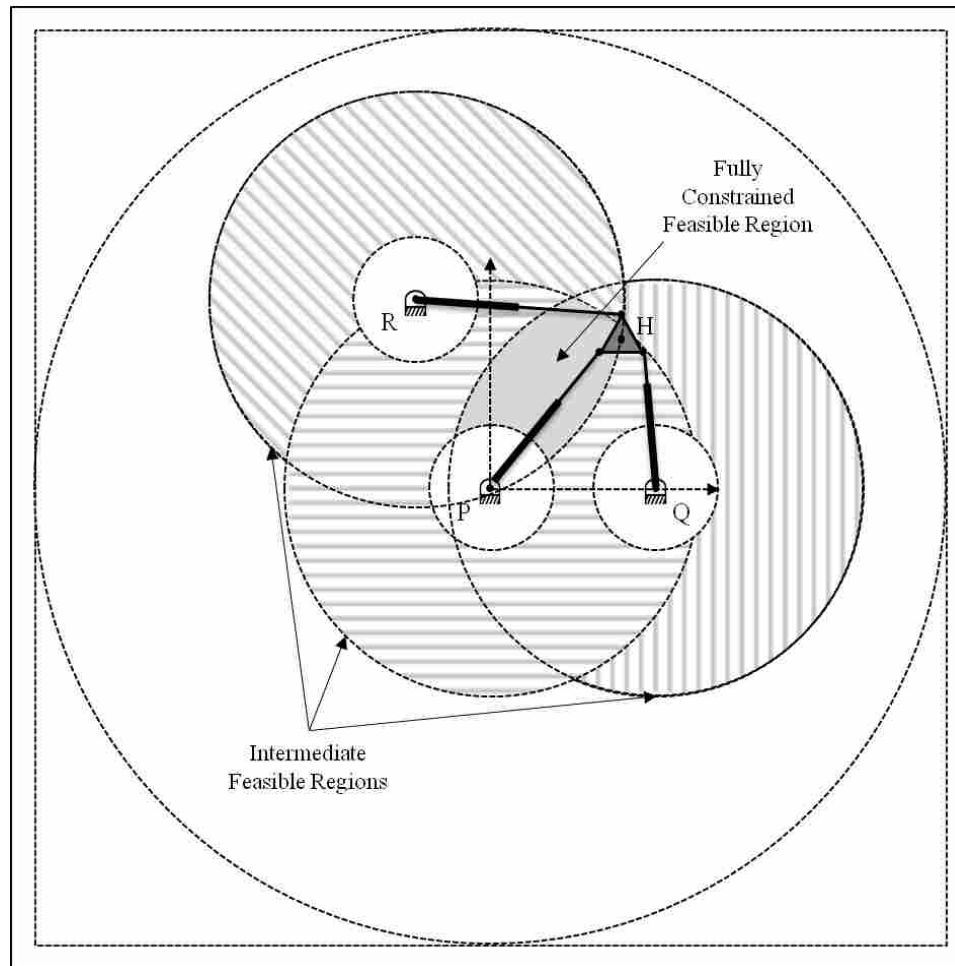


Figure 3-11: One Fully Constrained Design

The manipulability is measured given the handle and joint variables for each location of the handle through a given ϕ_{Range} . The manipulability measure, ω , is found by taking the determinant of the Jacobian at each handle placement as discussed in the previous chapter. Thus, a manipulability map is created for each design. As an example, Figure 3-13 contains a fictitious manipulability map for the square post-constraint sample region shown in Figure 3-12. To value a design the manipulability map must be investigated for singularities. This is covered in the next section.

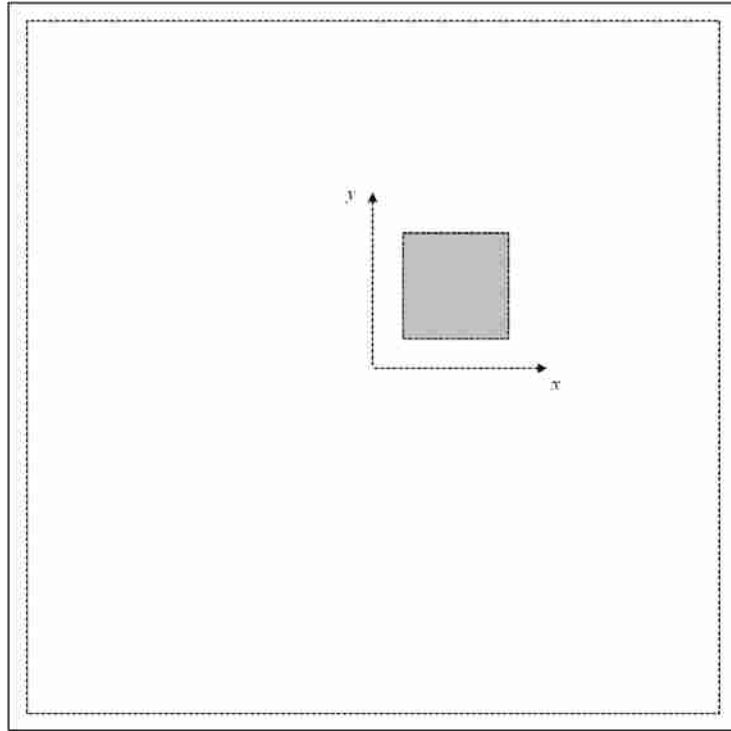


Figure 3-12: Post-Constraint Sample Region to be Measured

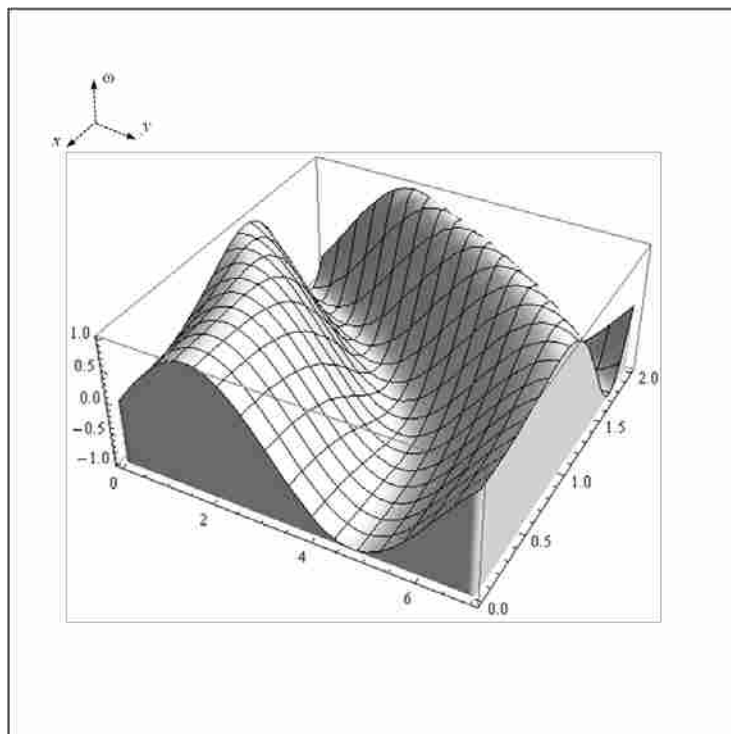


Figure 3-13: Manipulability Map of Post-constraint Sample Region

3.4 Identification and Separation of the Workspaces

The manipulability map is used to determine workspaces, which are regions in the manipulability map that do not contain singularities. A computer algorithm is used to identify each workspace in the manipulability map for each design. The algorithm discovers regions surrounded by singularities. Ill-conditioned values are treated as singularities. Prior to optimization the designer sets a manipulability tolerance that defines which ranges of manipulability around the value of zero are considered to be singularities. Singularities exist where the measure of manipulability, ω is equal to zero. To divide a work region into workspaces a slice is taken across the zero plane, as shown in Figure 3-14.

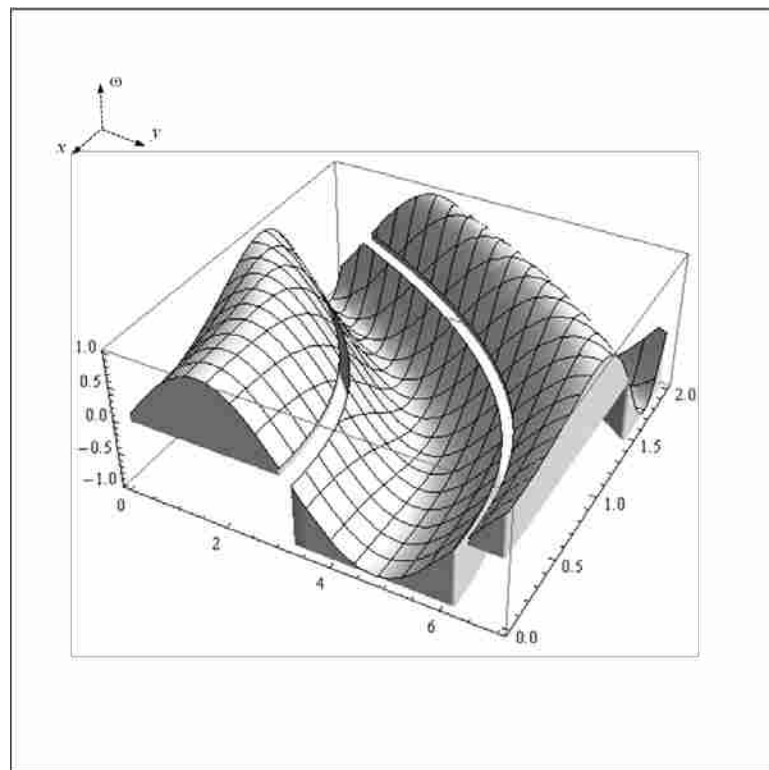


Figure 3-14: Singularity Discovery in the Manipulability Map

Each workspace is identified by using the zeros in the manipulability map as dividers. The work region is then split into several workspaces separate from each other, as shown in Figure 3-15, so that they can be characterized and compete against each other and all other workspaces that come from the other designs.

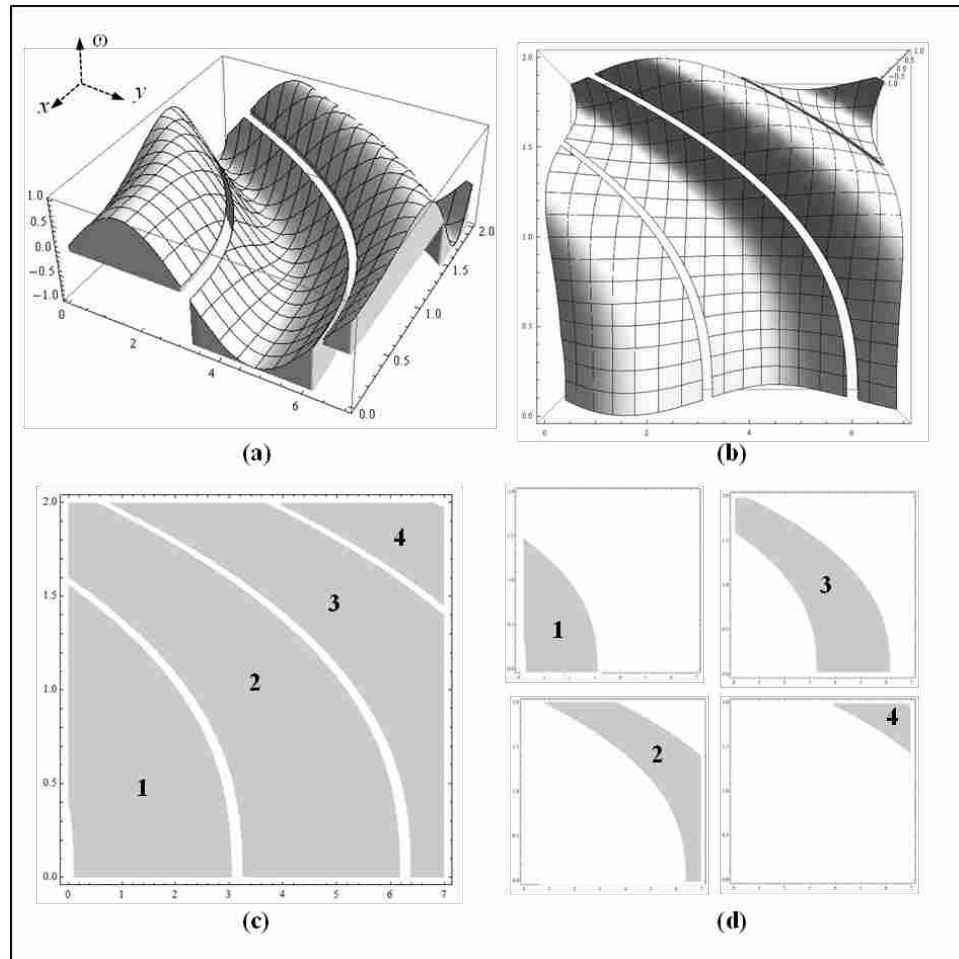


Figure 3-15: Identification and Separation of Workspaces

3.5 Characterization of Workspaces

Once workspaces are identified and separated from other workspaces, they must be characterized. Workspaces are characterized based on four measures: area, compactness,

average manipulability and standard deviation of manipulability. Each of these measures aid the designer in the selection of an ideal workspace. Area ensures a sufficient workspace size. Compactness, defined as the square of the perimeter divided by the area, is a measure of the shape of the workspace: the lower the compactness score, the more it resembles a circle, as illustrated in Figure 3-16. A high average manipulability is desired for haptic applications to ensure adequate force and torque capabilities in all directions. The standard deviation of the manipulability is important to ensure that the average manipulability score is meaningful. It is possible for a workspace to contain a high average manipulability but not have an even distribution. A small area of extremely high manipulability values could create a large “spike” pulling the mean manipulability higher than the rest of the sample. The goal is to have a high manipulability while still maintaining a relatively even distribution across the workspace surface; to this end the average manipulability and the standard deviation of manipulability are used as design objectives.

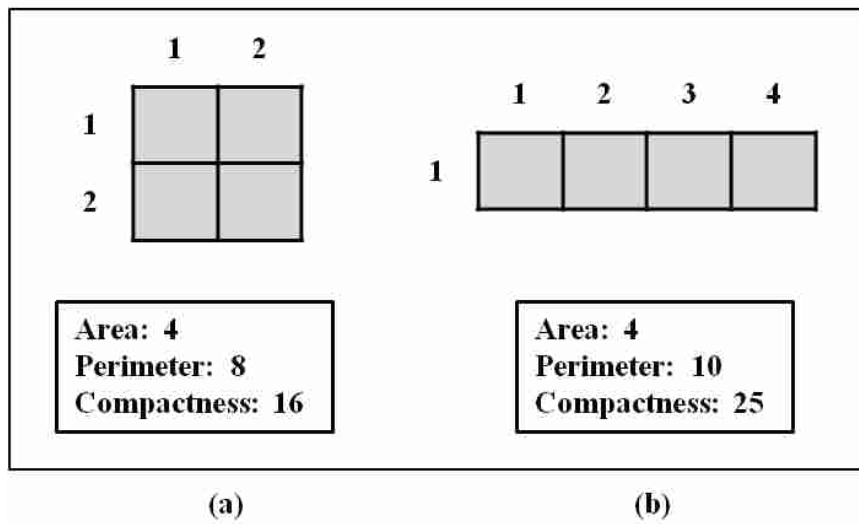


Figure 3-16: Understanding Compactness

As the workspaces are irregular and composed of discrete points, an approximation of their area and perimeter is made. The area score is determined as the number of discrete points in the workspace. Similarly, the perimeter is the number of points around its edges. These points are used throughout the test and are converted to standard measurements just before selecting a final design. See Figure 3-17.

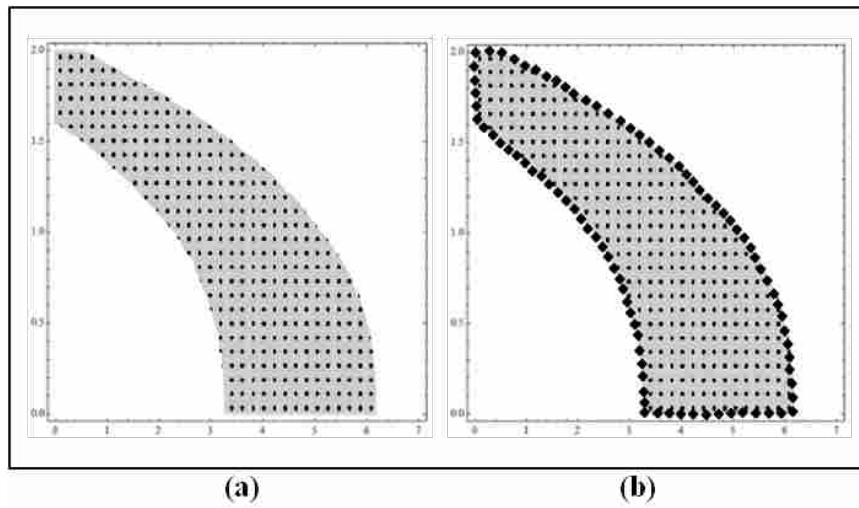


Figure 3-17: Area and Perimeter Derivation

3.6 Workspace Optimization

Once the workspaces have been mapped, separated, and characterized they are ready to be compared to each other. There are a number of different ways to approach this optimization problem. The optimal workspace is found by maximizing area and average ω while minimizing compactness and standard deviation of ω . For ease of implementation this problem is turned into a minimization problem by multiplying area and average ω by -1. Thus, the optimization

problem is defined as a minimization of the four design objectives: -area, compactness, -average ω , and standard deviation of ω .

3.6.1 Optimization Problem Statement

This section contains the formal optimization statement. The statement is written generally so that a designer can follow the statement using an optimization tool of their choice. Following the explanation, the author will demonstrate one such tool to solve the optimization problem.

Definitions

T represents a threshold

* indicates the optimal design for a sub tournament

$H = \begin{bmatrix} x_{H_1} & y_{H_1} \\ x_{H_2} & y_{H_2} \\ \vdots & \vdots \\ x_{H_{n_{\tilde{H}}}} & y_{H_{n_{\tilde{H}}}} \end{bmatrix}$ is the set of all handle placements that will be explored

\tilde{H} is a subset of H based on constraints

λ is calculated as the number of points in \tilde{H}

ρ is calculated as the number of perimeter points in \tilde{H}

$\zeta = \frac{\rho^2}{\lambda}$ is a measure of shape compactness

$$\bar{\omega} = \frac{1}{n_{\tilde{H}}} \sum_{i=1}^{n_{\tilde{H}}} \omega_i$$

$$\sigma = \sqrt{\frac{1}{n_{\tilde{H}}} \sum_{i=1}^{n_{\tilde{H}}} (\omega_i - \bar{\omega})^2}$$

Problem Statement

$$\min_{x_Q x_R y_R} [-\lambda \zeta - \bar{\omega} \sigma]$$

Subject to:

$$x_Q \leq 2 * d_{max} + h_2$$

$$-(2 * d_{max} + h_1) \leq x_R \leq 2 * d_{max} + h_1$$

$$-(2 * d_{max} + h_1) \leq y_R \leq 2 * d_{max} + h_1$$

$$\lambda(\tilde{H}^*) \geq T_\lambda$$

$$\zeta(\tilde{H}^*) \leq T_\zeta$$

$$\bar{\omega}(\tilde{H}^*) \geq T_{\bar{\omega}}$$

$$\sigma(\tilde{H}^*) \leq T_\sigma$$

where

\tilde{H}^* is the \tilde{H}_i that has the largest value for S

where

\tilde{H}_i is the i -th continuous subset of H that satisfies

$$-(2 * d_{max} + h_1) \leq x_H \leq 2 * d_{max} + h_1$$

and

$$-(2 * d_{max} + h_1) \leq y_H \leq 2 * d_{max} + h_1$$

and

$$d_{min} \leq d_{j,\phi} \leq d_{max}, \quad \forall j \in \{1, 2, 3\}$$

$$\forall \phi \in \{\phi_{min}, \phi_{min} + \Delta\phi, \dots, \phi_{max}\}$$

and

$$\omega_{\phi}^2 - T_{\omega}^2 \geq 0, \quad \forall \phi \in \{\phi_{min}, \phi_{min} + \Delta\phi, \dots, \phi_{max}\}$$

and where

$$S = \frac{\lambda_H - \lambda_i(\tilde{H}_i)}{\lambda_H} - \frac{\zeta_H - \zeta_i(\tilde{H}_i)}{\zeta_H}$$

is the criteria for the selection of the optimal reduced set \tilde{H}_i for a given design.

$$d_1 = \sqrt{(x_H - e \cos(\phi + \alpha))^2 + (y_H - e \sin(\phi + \alpha))^2}$$

$$d_2 = \sqrt{(x_H - e \cos(\phi + \alpha) - x_Q + h_2 \cos(\phi))^2 + (y_H - e \sin(\phi + \alpha) - y_Q + h_2 \sin(\phi))^2}$$

$$d_3 = \sqrt{(x_H - e \cos(\phi + \alpha) - x_R + h_1 \cos(\phi + \alpha))^2 + (y_H - e \sin(\phi + \alpha) - y_R + h_1 \sin(\phi + \alpha))^2}$$

$$\omega = \text{Det} [J]$$

This formal optimization statement is the basis for the optimization method used in this thesis. This same method can be used with diverse optimization tools. One such tool, a series of Pareto filters, is employed to solve the optimization problem and can be seen in the subsequent section.

3.6.2 Pareto Filter Optimization

This multi-objective problem is solved by using a Pareto filter and a smart Pareto filter in succession. A brief discussion of these filters is given here; a detailed discussion of the Pareto filter and smart Pareto filter is given by Messac and Mattson [33] and Mullur et al. [34], respectively.

The goal of these filters is to reduce a large number of design options to a smart Pareto set. As stated in [34], “a smart Pareto set is one that is *small* and *effectively represents the*

tradeoff properties of the complete Pareto frontier.” See Figure 3-18. The workspaces selected in the smart Pareto set represent the best options from which the designer can select by inspection of the final design sets.

Figure 3-18 (a) illustrates the Pareto filter method. In this two-objective optimization example the goal is to find a set of designs that represent the minimization trade-off combinations of the design objectives, μ_1 and μ_2 . Figure 3-18 (b) shows different designs that have been generated. Each design has a unique combination of the design objectives. The darkened points in Figure 3-18 (c) are optimally Pareto. Each design shown is better in some way than all the lightly shaded designs. These Pareto points are found by subtracting one design vector from another and letting the champion remain. Although this method is often effective for small data sets an additional step must be taken for large sample sizes. Figure 3-18 (d) illustrates typical results obtained through the use of a smart Pareto filter. Two parameters, Δt and Δr , help the designer select a smaller number of samples from the Pareto set to examine. “The parameter Δt is primarily a design objective tradeoff parameter, which is used to remove points that are insignificantly different from others with respect to a given objective.” [34] “The parameter Δr is primarily a distribution/representation parameter, which is used to control the degree to which flat regions of the Pareto frontier are represented in the smart Pareto set.” [34] The remaining dark design points in Figure 3-18 (d) comprise the example set of smart Pareto designs. Note the depiction of Δt and Δr shown as the widths and lengths, respectively, of the shaded regions indicating eliminated Pareto points. The parameters Δt and Δr have physical meaning because they are relative to the distances between design objectives. To provide a uniformly representative set each design should have two Δt widths and two Δr lengths; this will allow a

designer to tune the optimization by relating Δt and Δr to the physical difference between design objectives.

This reduced set contains workspaces that represent trade-offs between the objectives, with each workspace possessing a different mix of these objectives; some emphasize one objective over another. It is up to the designer to select from this small list the mix of objectives that best meet the desired application. An example of such a selection would be to select a design that emphasized compactness then area followed by the other objectives.

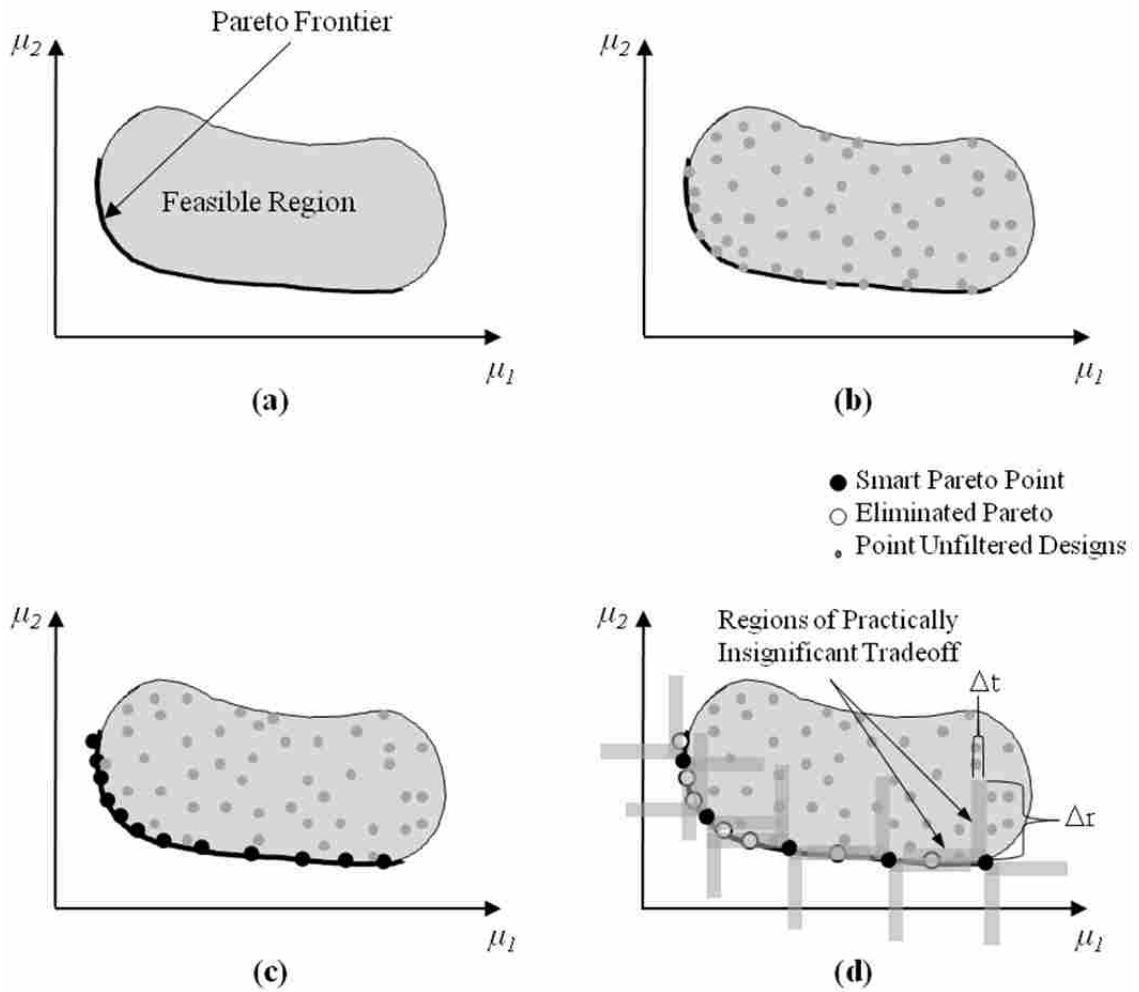


Figure 3-18: Pareto and Smart Pareto Filters

The filters map the characteristics of each of the design objectives, so that the designer can easily select this mix. The designer can choose to examine a subset of the objectives but to get the full optimization they will enter all the objectives. Compare the two-objective set to the four-objective set in Figure 3-19. In this illustrative example each design contains four design objectives $\boldsymbol{\mu} = [\mu_1 \mu_2 \mu_3 \mu_4]^T$. As four dimensions are difficult to visualize, four plots are drawn in each column with μ_1 as a baseline. In the first column each plot ignores design information and only focuses on two design objectives. The designs have been Pareto filtered and smart Pareto filtered. The small gray dots represent designs. The open circles represent points eliminated from the Pareto set and the remaining darkened points represent the set of smart Pareto optimal designs.

It is relatively easy to see and interpret the results of the filters. The column on the right, column b, is more challenging. Instead of ignoring design information, each plot takes into account all four design objectives; because the filters compare the total design vector local Pareto point seen in the first column are eliminated and only global points remain. As each plot is aligned with the first design objective μ_1 , a careful comparison of the two columns will reveal that two local Pareto points have been eliminated in the four-objective set in column b. The two-objective case is shown only for an illustrative purpose. Optimization of a manipulator takes into account all desired design objectives.

Note that before entering candidate designs into a Pareto filter it is perfectly acceptable to screen designs subject to some constraint. Figure 3-20 gives an idea of the number of designs that would not need to be processed if a threshold value had been applied to μ_1 . This threshold is applied as follows: minimize μ subject to constraint $\mu_1 < -100$. Thus, all designs on the right

hand side of the darkened threshold bar would never enter the optimization process. They are shown here only for illustration.

Each mix of tradeoffs is examined and one of the smart Pareto designs is selected. The corresponding design is composed of the base locations that produced the selected workspace that is optimally selected for manipulability considerations to yield high haptic performance. Such a design is represented generally in Figure 3-21.

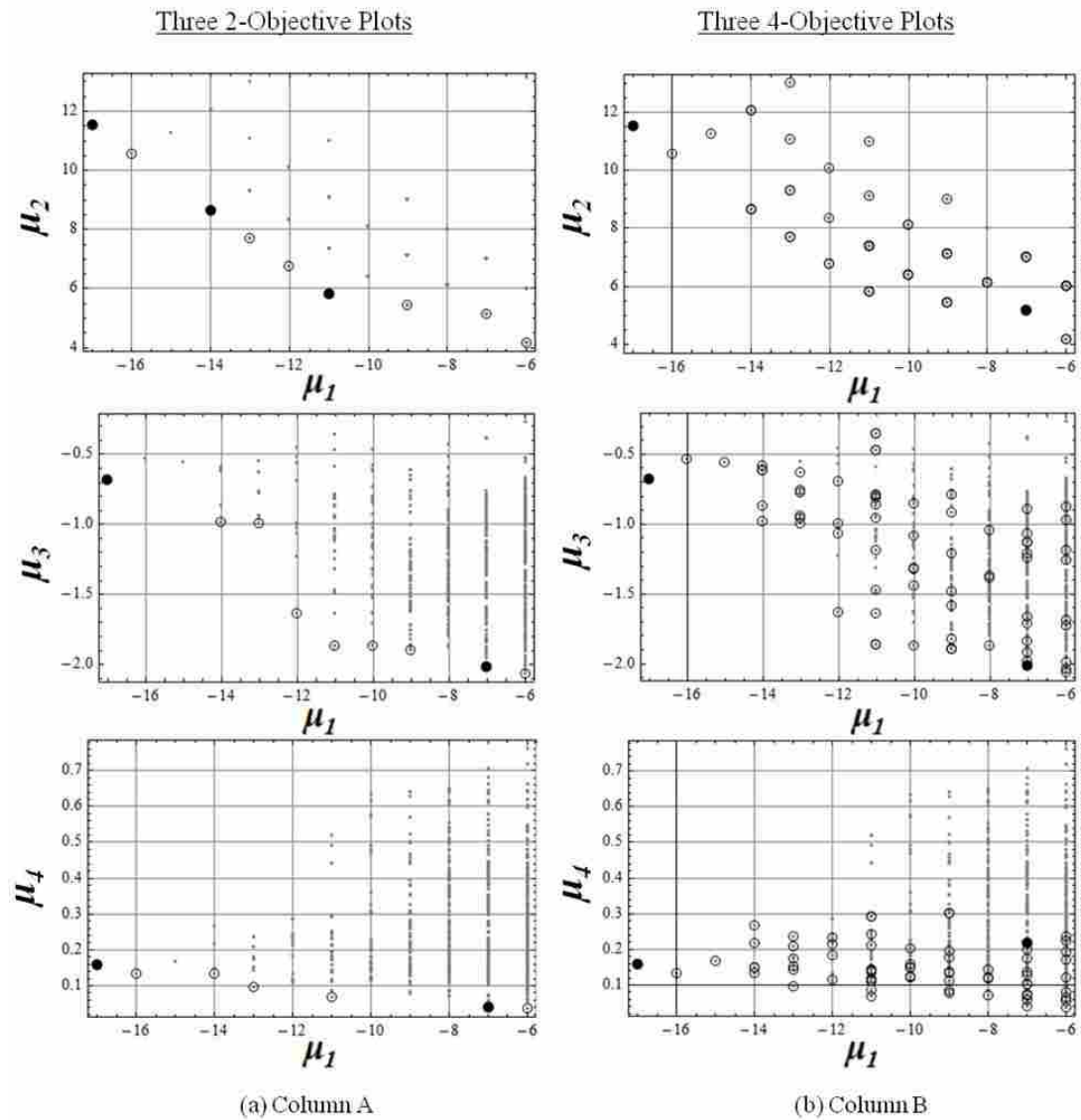


Figure 3-19: Visualization of Trade-offs and Filtered Designs

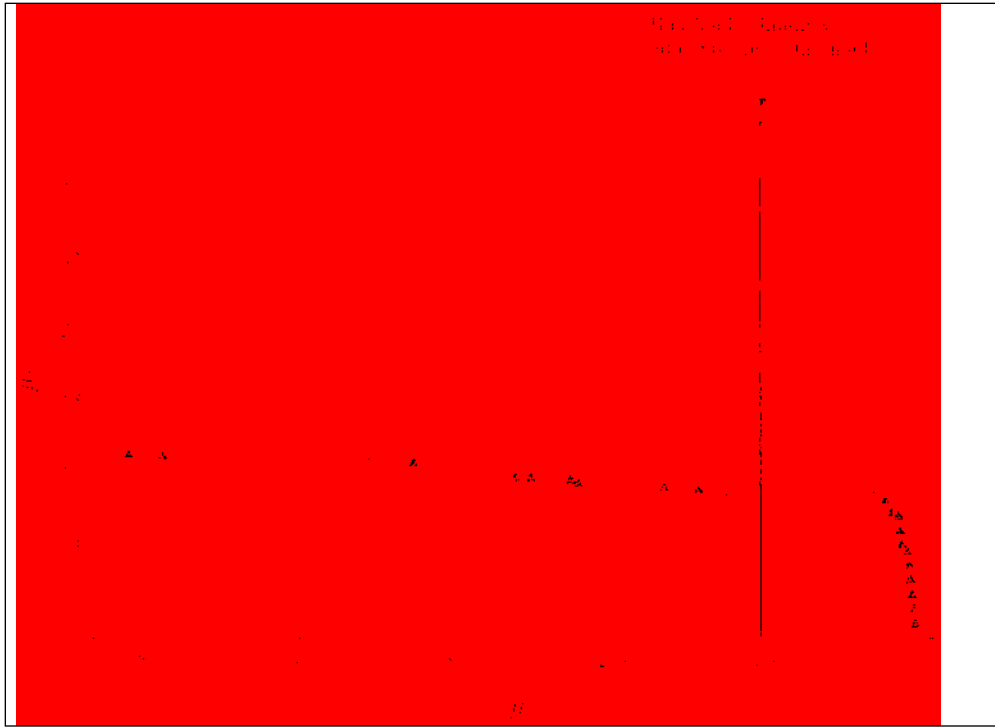


Figure 3-20: Reducing Designs Subject to a Constraint

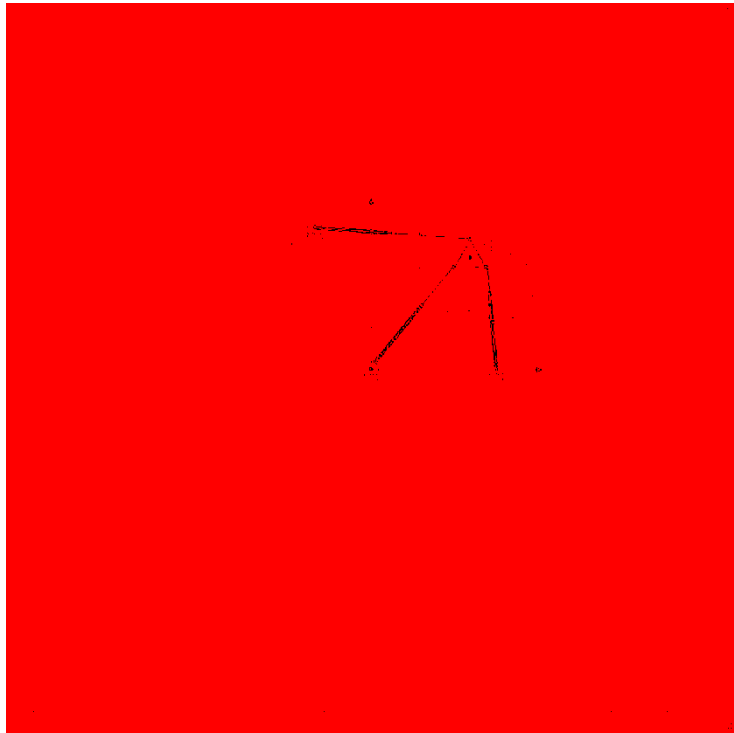


Figure 3-21: Representation of an Optimized Haptic Design Interface

3.7 Software: Optimization Algorithm Implementation

The algorithms used to find the optimal designs are coded and implemented in *Mathematica*, a math based software, by the author. Pareto filter and smart Pareto algorithms are adapted from *MATLAB* code created by [35] and implemented in *Mathematica* by the author.

4 RESULTS

The methods described in Chapter 3 were applied to the optimization of the planar parallel haptic interface. The design optimization was performed using the arguments shown in Table 4-1. As seen from these arguments, the handle plate was selected to be an equilateral triangle and the handle placement was centered within the equilateral triangle. Note that both of these parameters are soft coded and are easily adjusted.

Table 4-1: Geometry Arguments for Optimization

Geometry		
h_1	2.0	in.
h_2	2.0	in.
h_3	2.0	in.
α	30.0	degrees
d_{\min}	3.0	in.
d_{\max}	10.0	in.

Relevant settings chosen by the designer for the optimization are listed in Table 4-2. Note that only one value each is listed for Δt and Δr ; because Δt and Δr have physical meaning each design should have its own set of two Δt widths and Δr lengths to provide a uniform set. The use of only one Δt and Δr means that designs are eliminated without properly accounting for their physical meaning, hence these results are an approximation of a possibly more uniform set reduced with greater respect to physical meaning.

For the configuration explored here, the total computation time to generate the final eight optimal designs was 8 hours on a Dell XPS M1530, Intel® Core™2 Duo CPU T8300 @ 2.40 GHz processor. Most of the optimization algorithm runs very quickly. There are a couple of exceptions. It is very time consuming to obtain the manipulability map for every design. Also, to identify the workspaces the code requires that the manipulability map be binarized. After workspace identification and separation, the process of returning the manipulability values to the binarized manipulability map is the most time consuming.

Table 4-2: Optimization Settings

Optimization Settings		
Ill-conditioned Threshold	± 0.1	in.
ϕ Range	0.1 - 90.1	degrees
ϕ Resolution	1.0	degrees
Q Resolution	1.1	locations per in.
R Resolution	2.2	locations per in.
H Resolution	1.76	locations per in.
H Resolution Final	0.30	locations per in.
Δ^{1*}	0.0245	unitless
Δ^{r**}	10	unitless

*"The parameter Δt is primarily a design objective tradeoff parameter, which is used to remove points that are insignificantly different from others with respect to a given objective." [34]

**"The parameter Δr is primarily a distribution/representation parameter, which is used to control the degree to which flat regions of the Pareto frontier are represented in the smart Pareto set." [34]

The optimization progress is shown in Table 4-3. The algorithm tested 21,520 workspaces, and 20,919 candidate workspaces were eliminated because their area was less than the designer imposed threshold constraint. The 601 remaining designs were optimized with a Pareto filter, then this set of 72 workspaces was reduced to 8 smart Pareto optimal workspaces. The smart Pareto filter ensures that the mix of characteristics contained in each design vector

will differentiate it from the other final workspaces. Note the use of the terminology workspaces rather than designs as each of the vectors contained information on the workspaces; there can be more than one workspace to a design but only one design to a workspace. As it turns out the final eight workspaces have unique designs and this set of eight is referred to as designs in this section.

Table 4-3: Filtered and Optimized Designs

Design Results		
Designs Pre-Threshold	21,520	Workspaces
Designs Post-Threshold	601	Workspaces
Globally Pareto Optimal	72	Workspaces
Smart Pareto	8	Workspaces

The Pareto Filter and Smart Pareto Filter results are shown in Figure 4-1. As this is a four-objective optimization it is more difficult to visualize the minimization that occurs. The area score is used as a baseline to view each of the other objectives. The problem is set up so that all objectives are minimized. Note that as the area score is minimized, compactness and average manipulability worsen. Also note that the filter does not select local Pareto points but minimizes the whole design vector.

The final eight designs are examined in detail by the designer. The designer exams the approximate area and shape of each workspace in the 2D plot shown in Table 4-4. In the same table the height of the 3D plot gives the designer an indication of average and standard deviation of the manipulability measure. The figures on the left show the resulting workspace for each of the designs. The figures on the right show the manipulability for each design.

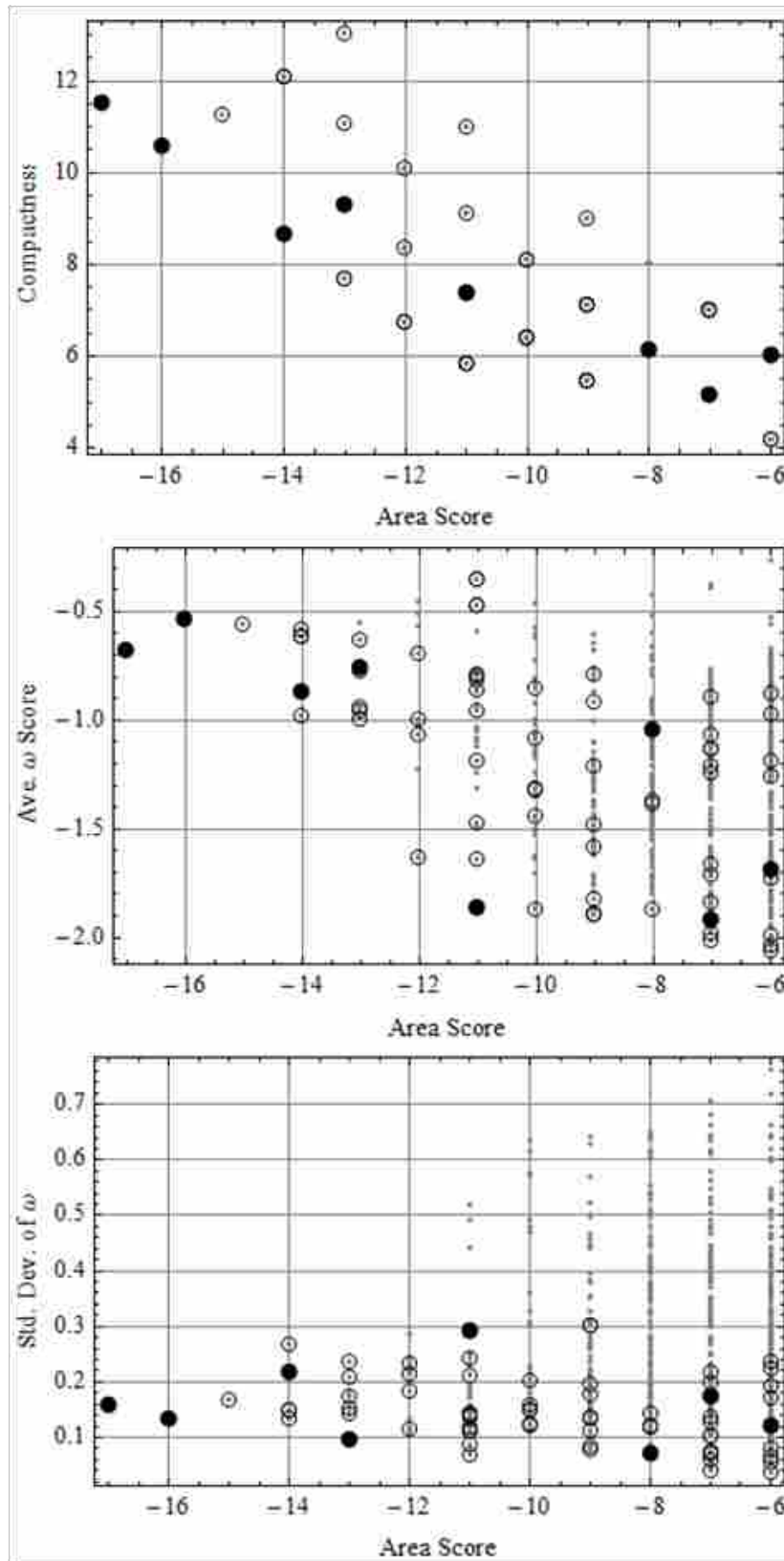
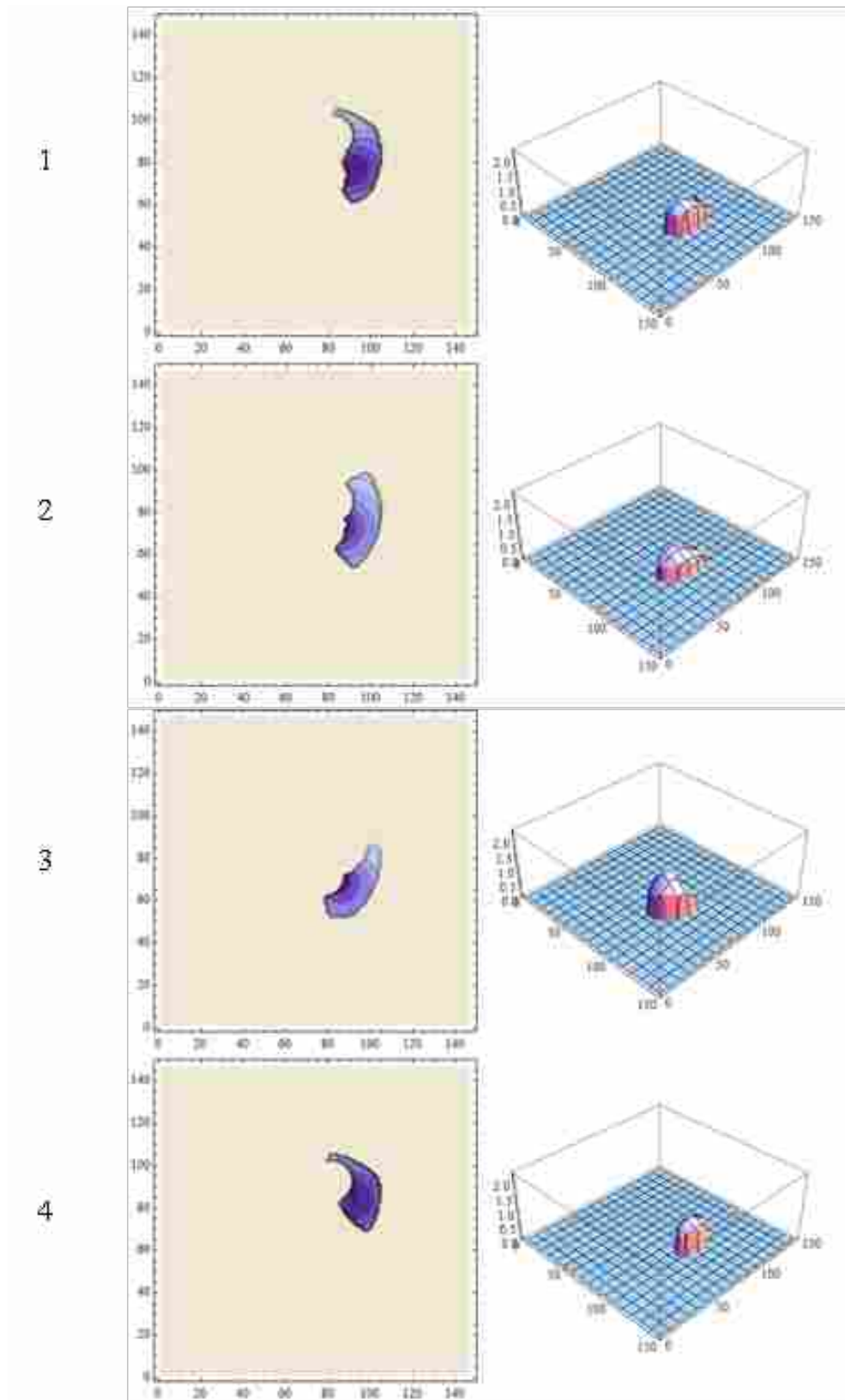
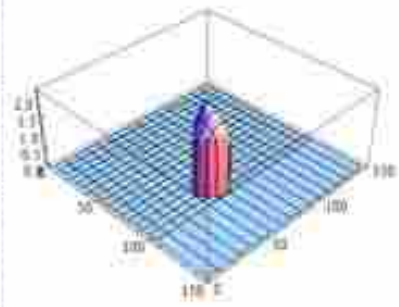
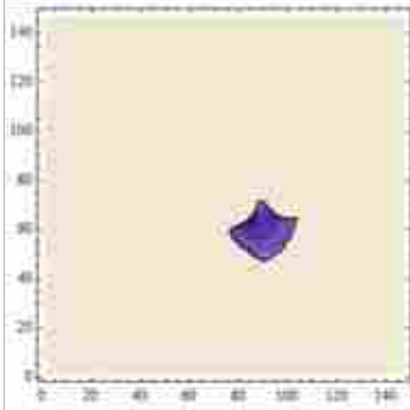


Figure 4-1: Pareto and Smart Pareto Filter Results

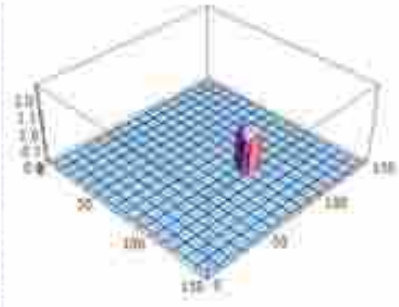
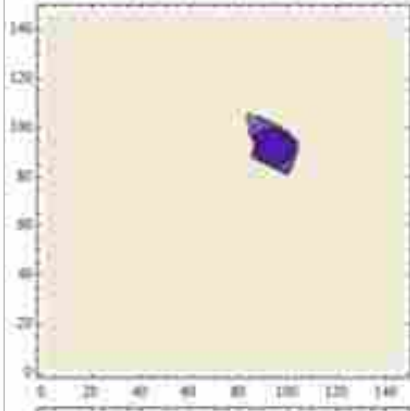
Table 4-4: Visualization of Filtered Designs



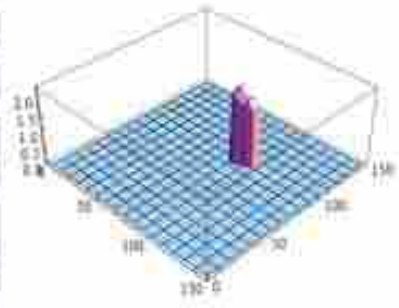
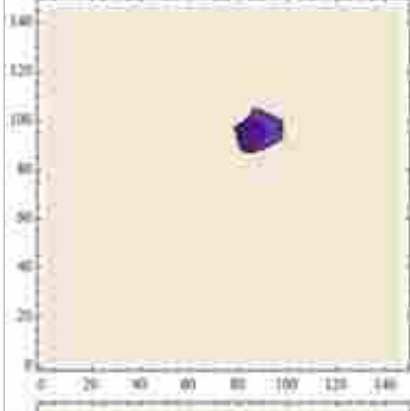
5



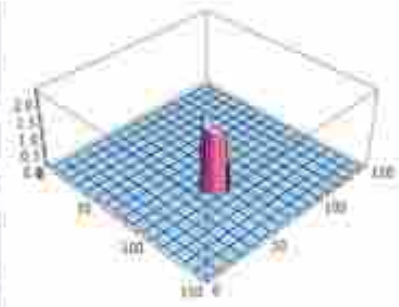
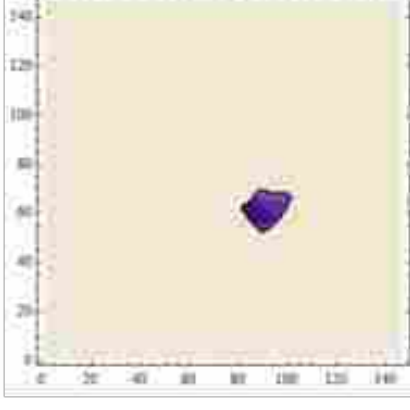
6



7



8



The plots shown in Table 4-4 aid the designer in the selection of a final design. However, closer inspection of the characteristics is required and can be seen in Table 4-5. The shaded areas indicate the minimum for each characteristic.

Table 4-5: Characteristics of Filtered Designs

Design	Area Score	Compactness	Mean ω Score	Std. Dev. ω
1	-536	19.0	-0.68	0.15
2	-562	15.4	-0.51	0.13
3	-435	15.8	-0.88	0.22
4	-425	19.1	-0.76	0.11
5	-347	11.8	-1.93	0.20
6	-284	13.1	-1.03	0.10
7	-222	10.4	-1.95	0.15
8	-201	9.6	-1.70	0.17

The information in Table 4-5 can be better understood as a decimal value shown in Table 4-6. In each column the score indicates how close it is to the best value of the eight for that individual characteristic, which is shaded. As each of these designs is optimized a designer can feel comfortable picking any of them, however, the designer may be looking for a particular set of design characteristics. One way to look at these designs is in terms of a total score. It should be stressed that this does not mean that the better score means a better design but it just includes the design that yields the highest combined score. Each score of the four characteristics is grouped into one score and then compared to the other eight. The “best” of these scores is shaded under the Trade-Off Score column in Table 4-6 and the rank of these scores is shown to its right. This table is given only as a guide to aid the designer’s selection. The decision of which mix of characteristics is optimal remains with the designer.

Table 4-6: Characteristics as a Percentage of Filtered Design Winners

Design	Area Score	Compactness	Mean ω Score	Std. Dev. ω	Trade-Off Score	Rank
1	0.95	0.51	0.35	0.69	0.84	7
2	1.00	0.63	0.26	0.82	0.91	5
3	0.77	0.61	0.45	0.47	0.77	8
4	0.76	0.50	0.39	0.97	0.88	6
5	0.62	0.82	0.99	0.51	0.98	2
6	0.51	0.74	0.53	1.00	0.93	4
7	0.40	0.93	1.00	0.66	1.00	1
8	0.36	1.00	0.87	0.61	0.95	3

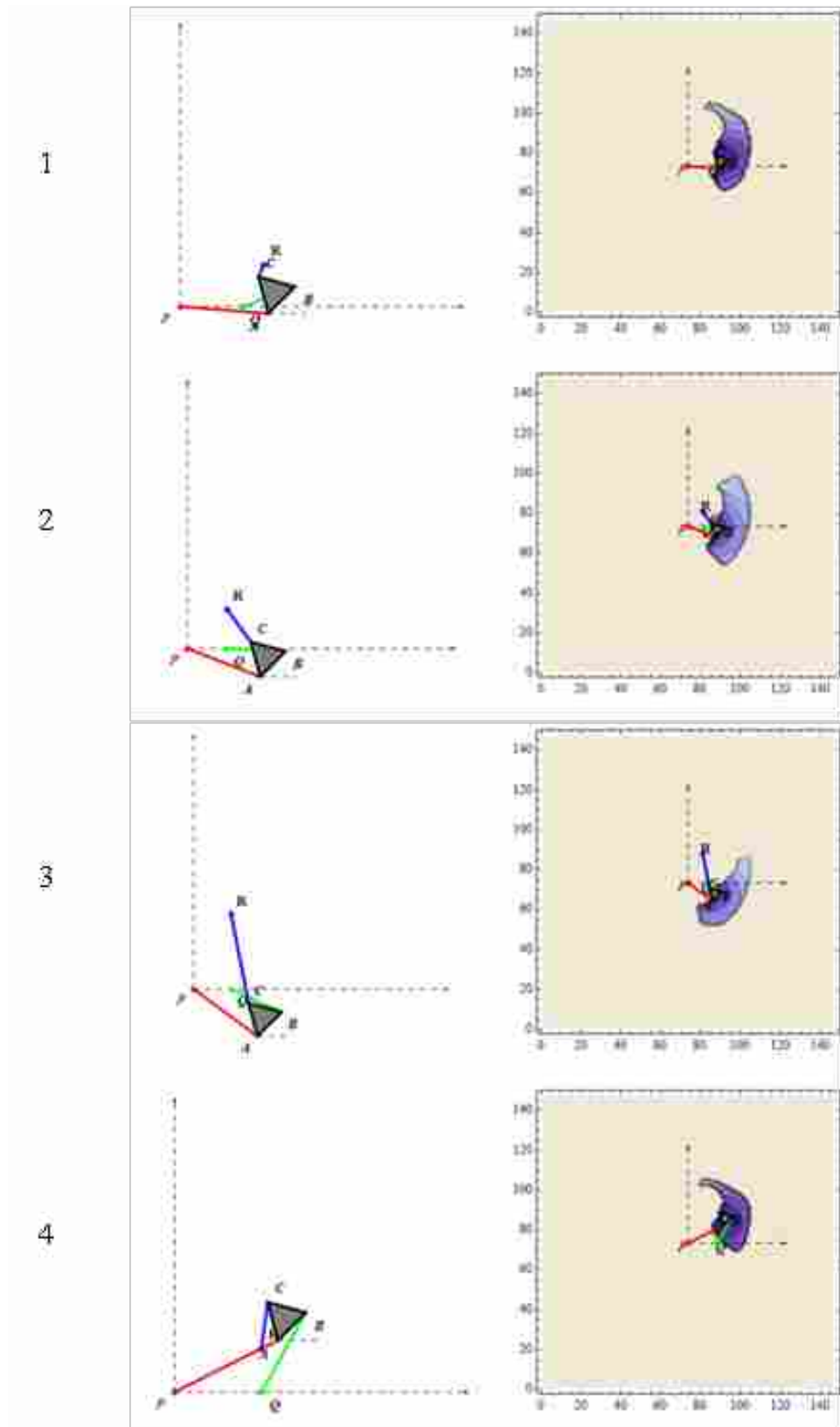
As a designer decides on a design it is helpful to know the approximate area of each workspace. This information can be used to determine which trade-off is acceptable. An approximate area for each design is shown in Table 4-7, along with the dimension of the side of a square with the same area.

Table 4-7: Design Area Values

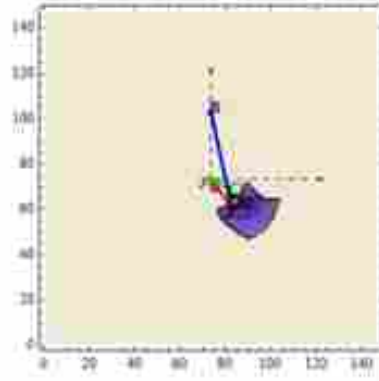
Design	Area in. ²	Sqrt(Area) in.
1	67.1	8.19
2	70.3	8.38
3	54.4	7.38
4	53.2	7.29
5	43.4	6.59
6	35.5	5.96
7	27.8	5.27
8	25.2	5.02

A designer may have a preference on a final design based on the specific locations of the design variables, bases Q and R . A visualization of each design is shown in Table 4-8. The figures on the left show the placement of the base points for each design. The figures on the right show the corresponding workspace.

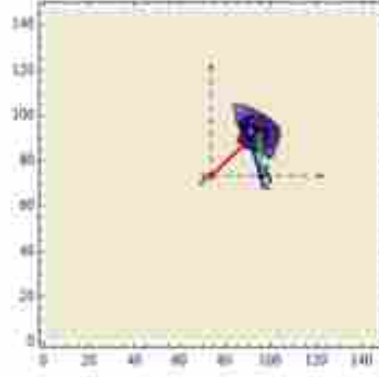
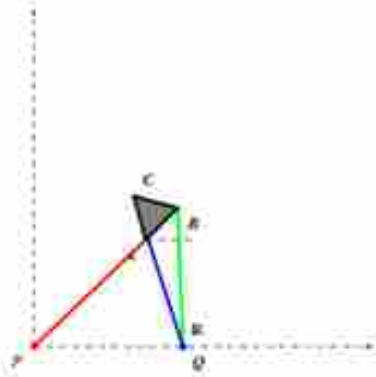
Table 4-8: Visualization of Design Configurations.



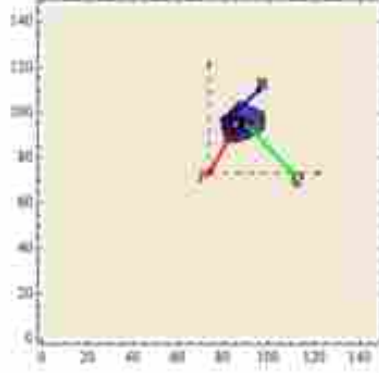
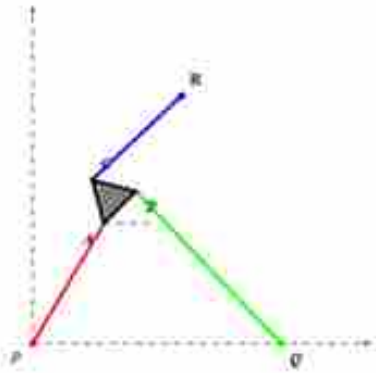
5



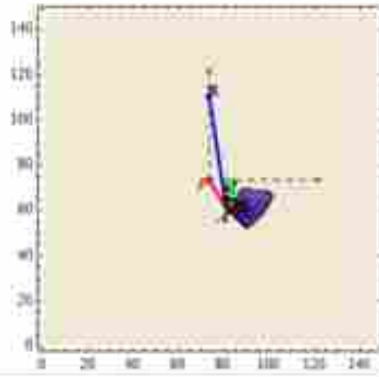
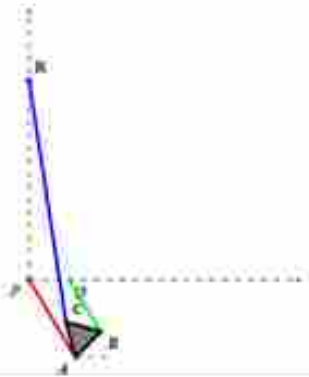
6



7



8



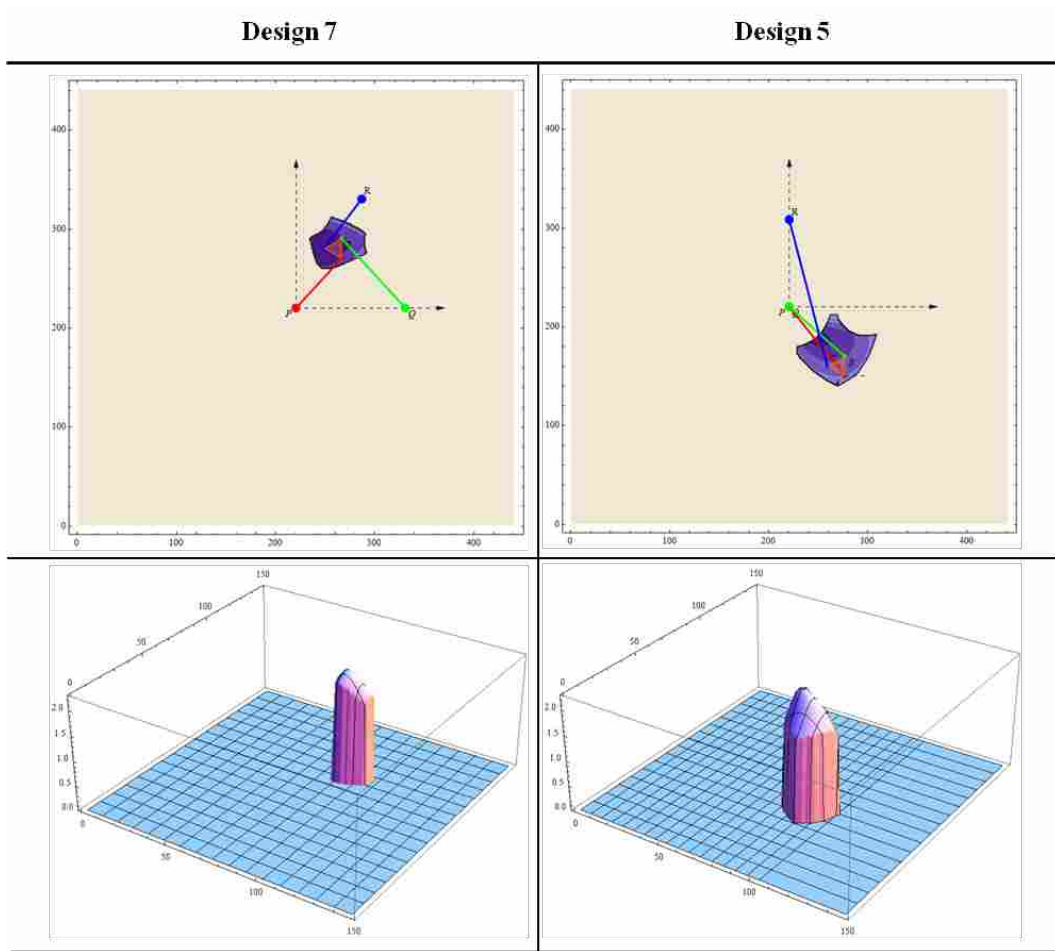
The specific base point locations for the eight final designs are summarized in Table 4-9.

Table 4-9: Design Configuration Data

Design	Position Q_x	Position R_x	Position R_y
1	3.3	4.4	2.2
2	2.2	2.2	2.2
3	2.2	2.2	4.4
4	4.4	4.4	2.2
5	0.0	0.0	8.8
6	6.6	6.6	0.0
7	11.0	6.6	11.0
8	2.2	0.0	11.0

A designer may have other design objectives that were not captured in the optimization problem. They can choose to formally incorporate them or they may want to use them as general guidance in the selection of a design. Table 4-10 shows two of the final eight designs that had a mix of characteristics that the designer found favorable. Design 7 has very good characteristics, namely compactness, average manipulability, and standard deviation of manipulability. These good scores come at the cost of workspace area. Design 5 has scores similar but lower than Design 7, however, it has the advantage of a larger workspace. It is really a designer's decision as to which is the better workspace. Additionally, a designer may inspect the placement of the bases and feel, for instance that Design 7 would provide a more stable manipulator once constructed. On the other hand, Design 5 may be preferred because it can be designed so that the bases are all far from the user. This selection depends on the application and is ultimately up to the designer.

Table 4-10: Closer Look at Two Selected Designs



5 DISCUSSION AND CONCLUSIONS

5.1 Discussion

The purpose of this thesis is to explore a general method to optimize the design of parallel haptic interfaces. The intent of such an optimization is to create devices that will allow users to participate in a more realistic haptic experience. Use of parallel devices can overcome such obstacles as low force, low torque, and low bandwidth, all of which reduce the experience of a user. The challenges that face designers of such devices are frequent encounters with singularities and low manipulability. This work has shown a method to overcome these problems by optimizing the design of an interface with respect to manipulability. A design is selected by finding a workspace that has the best manipulability characteristics associated with an acceptable size and shape.

Before the characteristics of each workspace could be measured they had to be divided into individual workspaces from the manipulability map. This process was not trivial and was accomplished by writing several algorithms that employed the use of specialized image processing applications from Wolfram's Mathematica software. These applications were able to identify points that were isolated by ill-conditioned and singularity values represented by zeros on the manipulability map. Once the workspaces were separated they could be characterized and compared in an optimization routine.

Characteristics should be selected based on the application of the device. The 3-RPR device design discussed in this thesis was optimized primarily with respect to manipulability, however, other design characteristics were necessarily taken into consideration, such as area size and area shape. In fact, after the characteristics were found for each workspace, a constraint was employed to screen designs before they were optimized. No workspace with an area less than 24 in² was shown in the results. This was accomplished by minimizing subject to an area constraint that translated to no designs less than 24 in². As shown in Table 4-3 this single constraint decreased the number of designs from 21,520 to 601 reducing the processing time required for the multi-objective optimization.

A Pareto Filter and Smart Pareto Filter were chosen for the optimization approach to best capture the multi-objective nature of the problem. Simple weighted aggregate methods were rejected as they left room for error in the optimization and required arbitrary selection of weights on the various measures. The designer can select the number of final designs shown by altering the optimization settings. The author set the filters to leave the top eight designs. Inspection of the designs showed that the trade-offs were sufficiently captured in eight designs to the author's satisfaction.

After close inspection of the final eight designs the author debated between the top two ranked designs shown in Table 4-10. Design 5 represented a great mix of design objectives with a high workspace area, however, the author favors Design 7 if the area is sufficient for the desired application, for its good combination of design objectives.

5.2 Conclusions

This research details development of a general method used to select an optimal design for a haptic interface with a parallel configuration. The method is demonstrated on a specific 3-

RPR parallel planar interface. Although this method is shown on only one device it can be applied to a variety of devices with adjustment. Arguments for each parameter can be adjusted, for example the minimum and maximum lengths of the joints or the dimensions of the handle. Optimization settings can be altered to change the results or to incorporate various design objectives. An example of such a change would be the inclusion of two unique Δt and Δr values for each design objective allowing for and incorporating better control over the physical optimization results. The extension of the method to other devices has its own set of challenges. One such challenge is that of determining the constraints. Even this planar example was quite complex when it came to the application of multiple constraints. Identifying constraints poses a significant challenge for complex systems with additional degrees of freedom.

A challenging portion of this algorithm is that of workspace identification and separation. This step represents considerable computation time and is accomplished with the aid of 3rd party software, *Mathematica*. It may be difficult to code this algorithm into a simpler language for greater efficiency.

The embodiment of this design will have its own hurdles. The forward kinematic equations produce multiple solutions and are dependent on an initial guess for the angle ϕ . The equations in this work assume that the manipulator is frictionless [2]. Although a design with a low standard deviation has been selected it will still be a challenge to ensure smooth operation of the actuated joints as the end-effector moves over a non-uniform manipulability workspace. This general method may need to be modified to capture additional information relevant to the optimization of a haptic device such as inertia, stability, resolution, tracking, stiffness, etc.

Design objectives were selected that enhance the haptic capabilities of the device. The method is designed to handle a selection of different or additional characteristics. If, for

example, a designer wished to select a different shape characteristic than compactness this could be readily achieved. The design constraints and design objectives are flexible.

The most important benefit of this method is that it enables the optimal use of parallel planar devices for haptic applications. The singularity avoidance and optimization with respect to manipulability techniques encompassed in the method enable haptic interfaces to better take advantage of the unique characteristics inherent in devices with a parallel configuration.

The method may be simplified by using a measure of the median rather than a combination of standard deviation and mean. The median is resistant to outliers and could present results in three dimensions rather than four. Additionally, a more even distribution of Pareto optimal designs could be obtained by normalizing the design characteristics before passing them through a series of Pareto filters.

One of the weaknesses of the method is that it does not make use of any “smart” algorithms as it maps the manipulability of an end-effector for a given design. The result is a computationally intensive approach. The computation time, limits the number of designs that can be searched and the resolution at which the selected designs can have their manipulability mapped. As this method is extended to more complex mechanism such as 6-DOF manipulators the need for faster processing times or a more efficient approach will increase. The algorithm could be coded into a more basic programming language to increase computation times. An alternate approach would be to incorporate a variable resolution. An algorithm could be written to identify regions that may be more promising and use a finer resolution.

The method effectively addresses the optimization goals for this thesis, namely: generation and optimal selection of designs based on singularity avoidance and manipulability. Other considerations included size, shape, and uniformity of manipulability over a workspace.

The equations derived in the thesis provided for determination of the velocities and static forces of the interface. These achievements progress the work towards the optimization of a haptic interface. To fully optimize a haptic interface, additional factors must be taken into consideration, notably the dynamics of the interface; these factors may include smoothness, stability, friction, inertia, interface specific concerns, etc. As a large part of haptic interface performance depends on these additional factors, the fundamental research in this thesis should be considered as a valuable first step towards full haptic optimization.

5.3 Future Research

The general method of optimization of haptic interfaces has a wide variety of applications. Extending work should include the construction of the 3-RPR parallel planar haptic interface optimized in this thesis. Valuable insight could be gained by physically proving out the design. Once constructed, a performance evaluation of the optimized parallel device can be conducted in human trials compared to serial and non-optimized parallel haptic devices.

A much broader field of haptics exists that includes 6-DOF devices; this general method should be explored for 6-DOF devices. Interfaces with 6-DOF could be greatly benefited by the strength and bandwidth available in devices configured in parallel.

Future work on the reduction of computation time is not trivial and is necessary for more complex devices. Haptic devices have gained recent use in handheld devices. Exploration of the uses of parallel haptic manipulators in this field could prove beneficial.

As previously stated this work is a step towards the full optimization of the haptic interface. This optimization groundwork provides a basis for optimization of additional factors. Future work should build on the body of this thesis to include optimization of the dynamics and

additional relevant design objectives to provide a fully immersive realistic haptic experience to a user.

REFERENCES

- [1] M. B. Colton, "Reality-based modeling of nonlinear passive devices for haptic simulations," University of Utah, Salt Lake City, UT, PhD Thesis ISBN: 978-0-542-79869-6, 2006.
- [2] L. Tsai, *Robot Analysis: The mechanics of serial and parallel manipulators*. New York, New York: John Wiley & Sons, Inc., 1999.
- [3] P. Ji and H. Wu, "An Efficient Approach to the Forward Kinematics of a Planar Parallel Manipulator With Similar Platforms," *IEEE Transactions on Robotics and Automation*, vol. 18, no. 4, pp. 647-649, August 2002.
- [4] H. Sadjadian and H.D. Taghirad, "Kinematic Analysis of the Hydraulic Shoulder: A 3-DOF Redundant Parallel Manipulator," in *Proceedings of the 2005 IEEE International Conference on Mechatronics & Automation*, July, 2005.
- [5] R. Unal, G. Kiziltas, and V. Patoglu, "A Multi-criteria Design Optimization Framework for Haptic Interfaces," in *Symposium on Haptic Interfaces for Virtual Environments and Teleoperator Systems*, Reno, Nevada, 2008, pp. 231-238.
- [6] G. A.V. Christiansson and E. C. Fritz, "A Novel Planar 3-DOF Hard-Soft Haptic Teleoperator," Delft Haptics Laboratory, Delft University of Technology, Delft, The Netherlands, 2007.
- [7] G. Campion, Q. Wang, and V. Hayward, "The Pantograph Mk-II: A Haptic Instrument," in *RSJ International Conference on Intelligent Robots and Systems*, 2005, pp. 723-728.
- [8] A. Frisoli, G. M. Prisco, F. Salsedo, and M. Bergamasco, "A Two Degrees-of-Freedom Planar Haptic Interface with High Kinematic Isotropy," in *International Workshop on Robot and Human Interaction*, Pisa, Italy, 1999, pp. 297-302.
- [9] L. J. Stocco, S. E. Salcudean, and F. Sassani, "Mechanism Design For Global Isotropy With Applications to Haptic Interfaces," in *Sixth Annual Symposium on Haptic interfaces for Virtual Environment and Teleoperator Systems*, Dallas, Texas, 1997.
- [10] R. L. Williams II and A. R. Joshi, "Planar Parallel 3-RPR Manipulator," in *Sizceth Conference on Applied Mechanisms and Robotics*, Cincinnati, 1999.
- [11] M. Zein, P. Wenger, and D. Chablat, "Singularity Surfaces and Maximal Singularity-Free Boxes in the Joint Space of lanar 3-RPR Parallel Manipulators," in *12th IFToMM World Congress*, Besancon, France, 2007.
- [12] H. Li, C. M. Gosselin , and M. J. Richard, "Determination of maximal singularity-free zones in the workspace of planar three-degree-of-freedom parallel mechanisms," *Mechanism and Machine Theory*, vol. 41, no. 10, pp. 1157-1167, 2006.

- [13] Y. Yang and J. F. O'Brien, "A Case Study of Planar 3-RPR Parallel Robot Singularity Free Workspace Design," in *International Conference on Mechatronics and Automation*, Harbin, China, 2007, pp. 1834-1838.
- [14] M. Gallant and R. Boudreau, "The Synthesis of Planar Parallel Manipulators with Prismatic Joints for an Optimal, Singularity-Free Workspace," *Journal of Robotic Systems*, vol. 19, pp. 13-24, 2002.
- [15] I. Tyapin, G. Hovland, and T. Brogardh, "Workspace Optimisation of a Reconfigurable Parallel Kinematic Manipulator," ABB Robotics, Vasteras, Sweden, 2007.
- [16] M. T. Masouleh and C. Gosselin, "Determination of Singularity-Free Zones in the Workspace of Planar 3-PRR Parallel Mechanisms," *Journal of Mechanical Design*, vol. 129, pp. 649-652, June 2007.
- [17] G. Alici and B. Shirinzadeh, "Optimum synthesis of planar parallel manipulators based on kinematic isotropy and force balancing," *Robotica*, vol. 22, pp. 97-108, 2004.
- [18] J. Lee, "A study on the manipulability measures for robot manipulators," *Proceedings of the 1997 IEEE/RSJ International Conference on Intelligent Robots and Systems*, vol. 3, pp. 1458-1465, September 1997.
- [19] K.L. Doty, C. Melchiorri, E.M. Schwartz, and C. Bonivento, "Robot manipulability," *IEEE Transactions on Robotics and Automation*, vol. 11, no. 3, pp. 462-468, June 1995.
- [20] P.A. Voglewede and I. Ebert-Uphoff, "Overarching framework for measuring closeness to singularities of parallel manipulators," *IEEE Transactions on Robotics*, vol. 21, no. 6, pp. 1037-1045, December 2005.
- [21] X. Liu, J. Wang, F. Gao, and L. Wang, "On the analysis of a new spatial three-degrees-of-freedom parallel manipulator," *IEEE Transactions on Robotics and Automation*, vol. 17, no. 6, pp. 959-968, December 2001.
- [22] C. Gosselin and J. Angeles, "The optimum kinematic design of a planar three-degree-of-freedom parallel manipulator," *ASME Journal of Mechanisms Transmissions and Automation in Design*, vol. 110, no. 1, pp. 35-41, 1988.
- [23] J. Wang and C. M. Gosselin, "Singularity Loci of a Special Class of Spherical 3-DOF Parallel Mechanisms With Prismatic Actuators," *Journal of Mechanical Design*, vol. 126, no. 2, pp. 319-326, March 2004.
- [24] X. Liu, "Optimal kinematic design of a three translational DoFs parallel manipulator," *Robotica*, vol. 24, no. 2, pp. 239-250, March 2006.
- [25] SensAble Technologies. (2009, December) SensAble Technologies Products & Services Web site. [Online]. <http://www.sensable.com/phantom-premium-1-5.htm>
- [26] J. C. Hong and R. Nakashima. (2009, Dec.) MSNBC. [Online]. www.msnbc.msn.com/id/16532335/
- [27] Force Dimension. (2010, February) Force Dimension. [Online]. <http://www.forcedimension.com/products>
- [28] F. Gosselin, J. Martins, C. Didard, C. Andriot, and J. Brisset, "Design of a New Parallel Haptic Device for Desktop Applications," in *First Joint Eurohaptics Conference and Symposium on Haptic Interfaces for Virtual Environment and Teleoperator Systems*, 2005.

- [29] K. Vlachos and E. Papadopoulos, "Transparency Maximization Methodology for Haptic Devices," *IEEE/SME Transactions on Mechatronics*, vol. 11, no. 3, pp. 249-255, June 2006.
- [30] C.M. Gosselin and J. Sefrioui, "Polynomial solutions for the direct kinematic problem of planar three-degree-of-freedom parallel manipulators," in *Fifth International Conference on Advanced Robotics*, Pisa, Italy, 1991, pp. 1124-1129.
- [31] T. Yoshikawa, *Foundations of Robotics: Analysis and Control*. Cambridge, Massachusetts: The MIT Press, 1990.
- [32] L. Tsai, *Robot Analysis: the mechanics of serial and prallel manipulators*. New York, United States of America: John Wiley & Sons, Inc., 1999.
- [33] C. A., Messac, A. Mattson, "Concept Selection Using s-Pareto Frontiers," *AIAA*, vol. 41, no. 6, pp. 1190-1198, 2003.
- [34] C. A. Mattson, A. A. Mullur, and A. Messac, "Smart Pareto Filter: Obtaining a Minimal Representation of Multiobjective Design Space," *Engineering Optimization*, vol. 36, no. 6, pp. 721-740, 2004.
- [35] C. A. Mattson, pareto_filter.m and smart_pareto_filter.m, Provided by Yearsley, Jonathan D.

